Static and Dynamic Analysis of Contrast Agents Parameter Estimates and the Effect of Constitutive Law

Dr. N. Pelekasis

Ph.D Thesis:	**Dr. Kostas Tsiglifis**
Post docs:	**Dr. M. Vlachomitrou**
Ph.D Candidates:	**K. Efthimiu, A. Litra**
MS Thesis: S.	**Serpetzi, T. Poteas**
Diploma Thesis:	**P. Dallas, N. Vorrias**

Funding: "HRAKLEITOS I , II" & "ARISTEIA" Programs, Greek Ministry of Education

Laboratory of Fluid Mechanics and Turbomachinery

Department of Mechanical Engineering

University of Thessaly, Volos GREECE

Invited Talk at the Dpt. Mechanical Eng., Imperial College London, March 6th 2013

Microbubbles (Contrast Agents)

- Bubbles surrounded by an elastic membrane for stability
- Low density internal gas that is soluble in blood
- Diameter 1 to 10 μm
- Polymer, lipid or protein (e.g. albumin) monolayer shell of thickness 15-200 nm

Motivation

- Contrast perfusion imaging $\Rightarrow$ check the circulatory system by means of contrast enhancers in the presence of ultrasound (Sboros et al. 2002; Frinking & de Jong, Postema et al., Ultrasound Med. Bio. 1998, 2004)
- Sonoporation $\Rightarrow$ reinforcement of drug delivery to nearby cells that stretch open by oscillating contrast agents (Marmottant & Hilgenfeldt, Nature 2003)
- Micro-bubbles act as vectors for drug or gene delivery to targeted cells (Klibanov et al, Adv. Drug Delivery Rev., 1999; Ferrara et al. Annu. Rev. Biomed. 2007)

- **Need for specially designed contrast agents**
  Controlled pulsation and break-up for imaging and perfusion measurements
- **Chemical shell treatment for controlled wall adhesion for targeted drug delivery**
- **Need for models covering a wider range of CA behavior (nonlinear material behavior, shape deformation, buckling, interfacial mass transport etc, compression vs expansion only behavior, nonlinear resonance frequency- thresholding)**
- **Need to understand experimental observations and standardize measurements in order to characterize CA's**

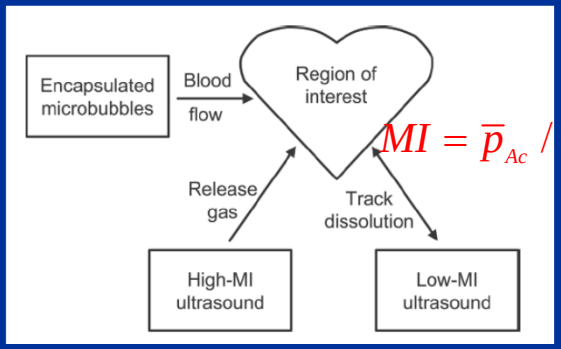

Contrast enhanced perfusion imaging, via a sequence of low and high Mechanical Index (MI) ultrasound pulses

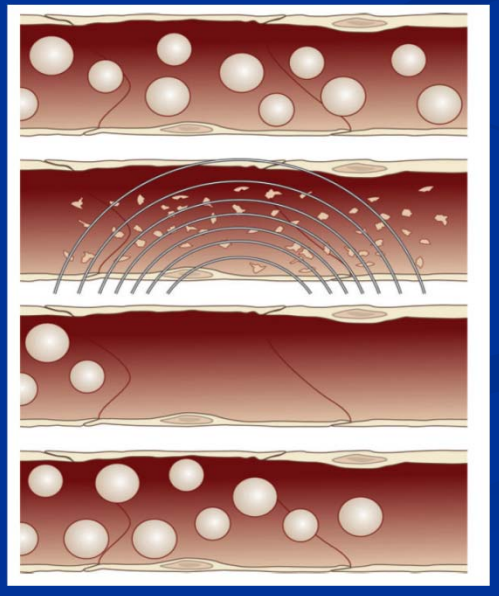

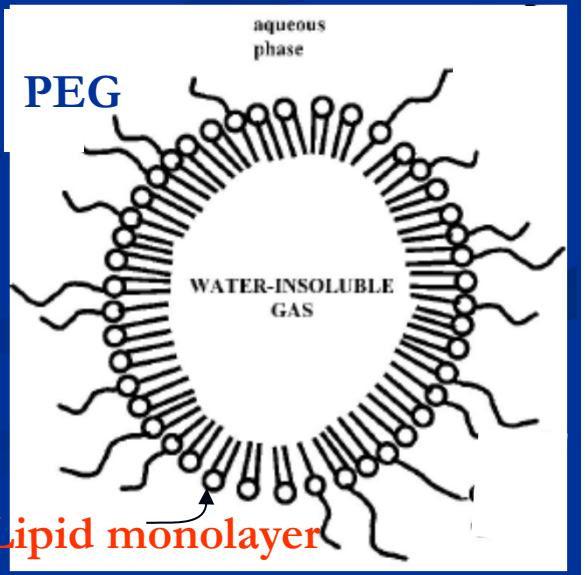

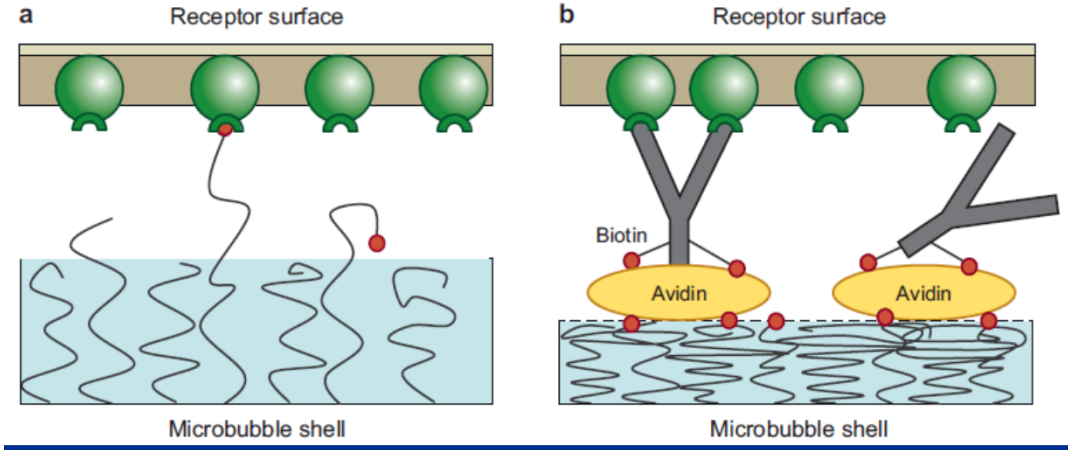

Ligand architectures. Cartoons show different schemes for the presentation of various ligand types: (*a*) small hydrophilic ligands can be covalently attached to the distal end of the carrier lipopolymer. The diffusion of the ligand is dictated by the polymer chain dynamics; (*b*) large, protein ligands can be attached by biotin (*red*) and avidin (*yellow*) linkage. The large size (60 kDa) and multiple binding pockets in the avidin create a sort of scaffold that is supported by the polymeric brush (2–5 kDa).

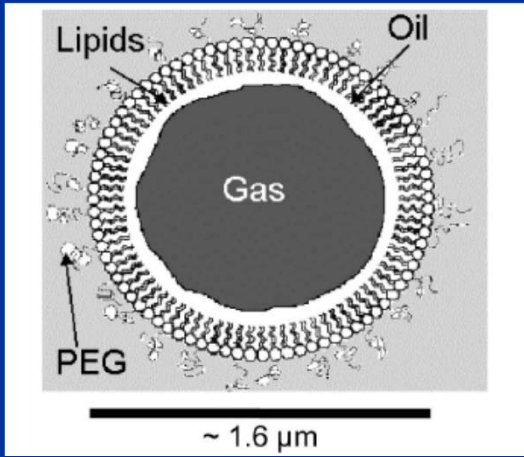

- Lipid monolayer shells are amenable to chemical manipulation for targeting and drug delivery
- Compound shell mechanical behavior not really known

Fig. 1. Schematic of an acoustically active liposphere depicting the location of the oil layer in which therapeutics can be dissolved, the lipid shell, and the gas interior (thickness of lipid/oil layer not to scale with diameter of AAL). The mean outer diameter of the AALs used in our study is 1.6 μm. The thickness of the oil and lipid layer was previously measured by May *et al.* [6], using scanning electron microscopy, and was found to be between 500 nm and 1000 nm, depending on the diameter of the entire agent.

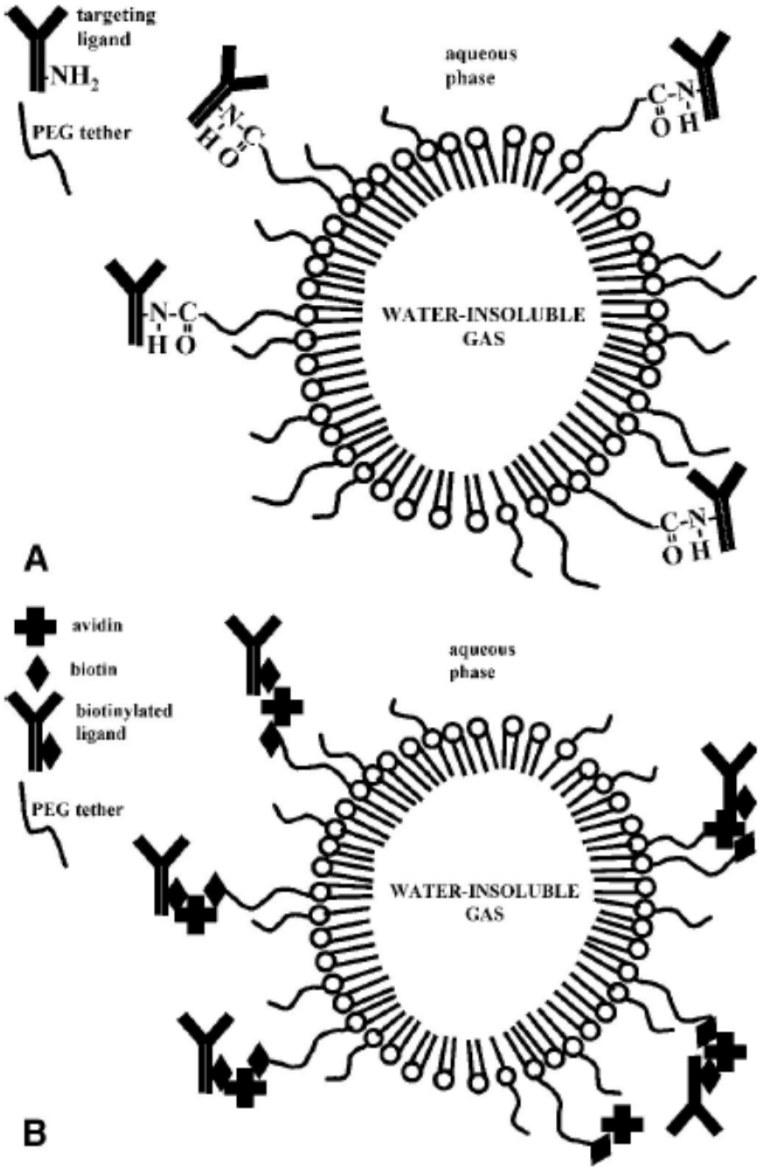

FIGURE 1. Covalent (A) or noncovalent (B) coupling of targeting ligands to the monolayer-coated gas microbubble via a flexible poly(ethylene glycol) spacer arm.

- Shell is important for designing and controlling the behavior of contrast agents

Phase Diagram

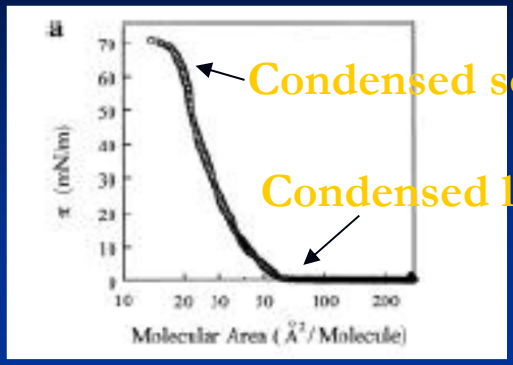

- Phase transitions occur as the available area per lipid molecule decreases, $\Pi = \gamma_0 - \gamma$

Π-A isotherms in a Langmuir trough

γ_0: surface tension of substrate

γ: surface tension of lipid surfactant monolayer

Wang et al. J. Phys. Chem. 1996

Static Response

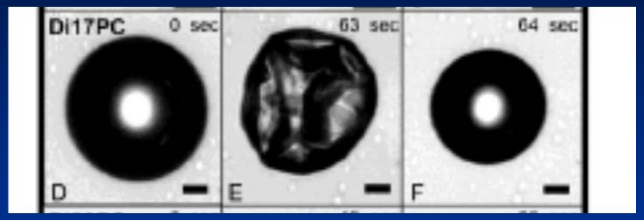

- They buckle when gas diffuses through the shell Borden & Longo, Langmuir 2002

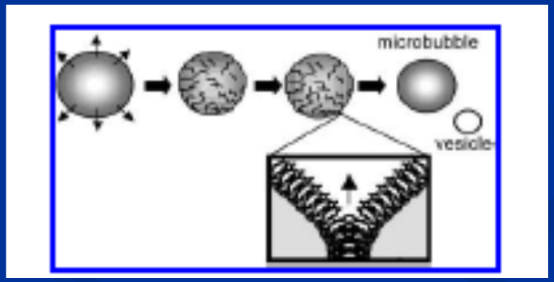

- They regain sphericity via a zippering mechanism that binds the hydrophobic tails of lipid monolayer

- Borden & Longo, Langmuir (2006→Shedding of excess lipids (**lipid shedding** or budding)
- Lee et al., Annu. Rev. Phys . Chem (2008)→ **Formation of bilayers** (reversibility)

Static Response during AFM Measurements

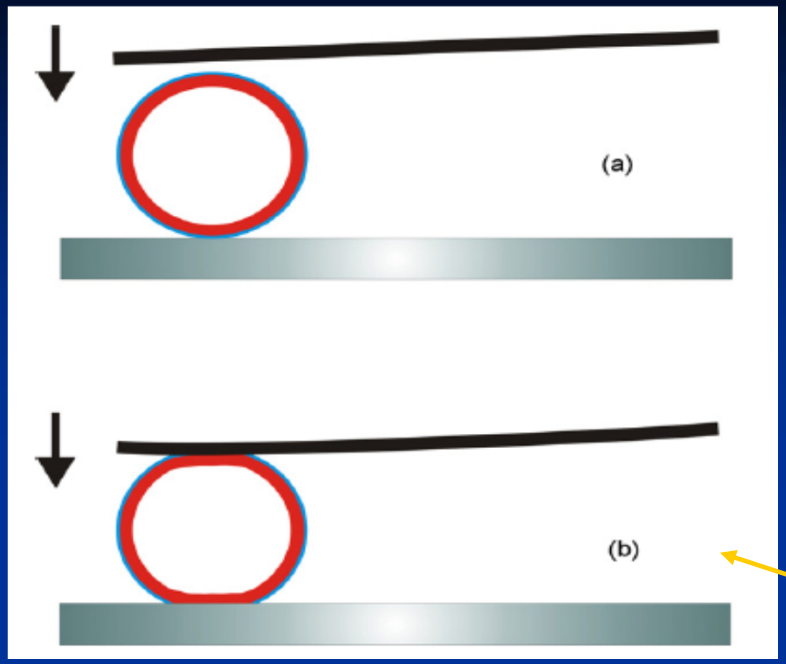

- Estimates of bending and stretching elasticities can be obtained based on AFM measurements of the static response of a coated microbubble
  (Ferry & Weinkamer, Polymer, 2007; Lulevich et al. J. Chem. Phys, 2004; Glynos, Sboros & Koutsos, Mat. Sci. Eng. B, 2009)
- Contrast agent with polymer and phospholipid shells are mainly examined

Schematic of an AFM setup for compression of single hollow microsphere with a tipless cantilever

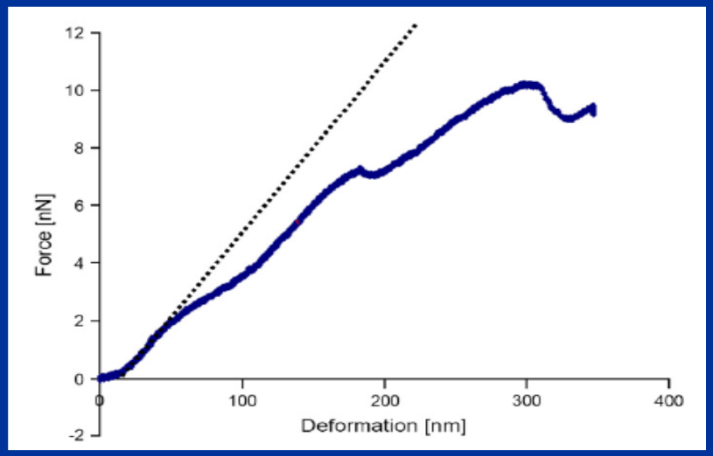

Experimental investigation of a water filled polysterene sulfonate capsule (PAH-PSS) (Ferry & Weinkamer 2007)

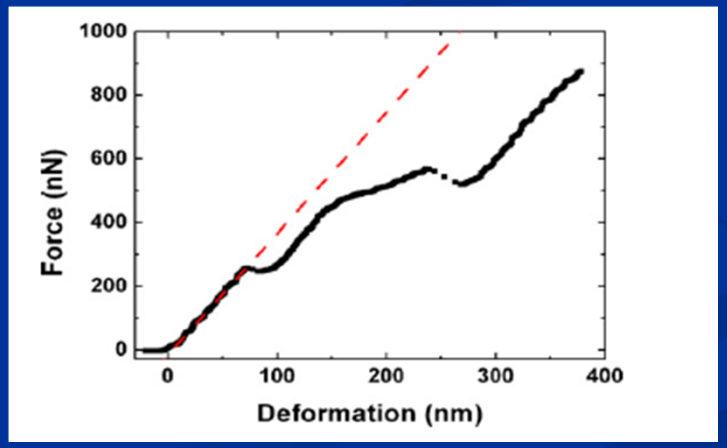

Experimental investigation of a polymeric thin-shell hollow microsphere (Glynos et al. 2009)

Provided the shell thickness is known Reissner's theory is used to fit the linear part for the shell stiffness

Need to identify the major force balances in different force ranges

Acoustic response of contrast agents

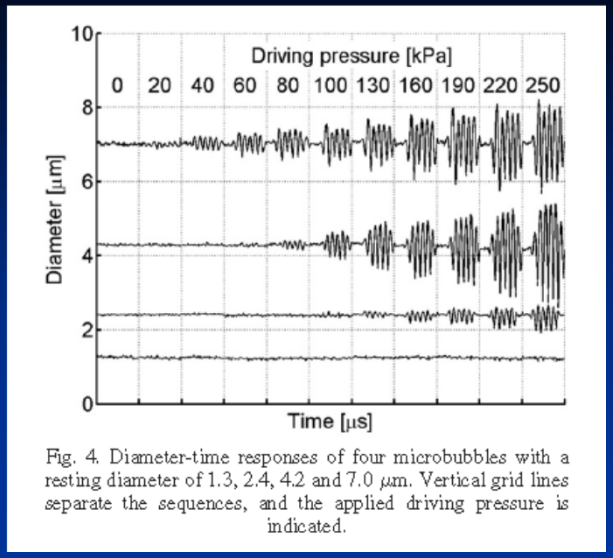

Fig. 4. Diameter-time responses of four microbubbles with a resting diameter of 1.3, 2.4, 4.2 and 7.0 μm. Vertical grid lines separate the sequences, and the applied driving pressure is indicated.

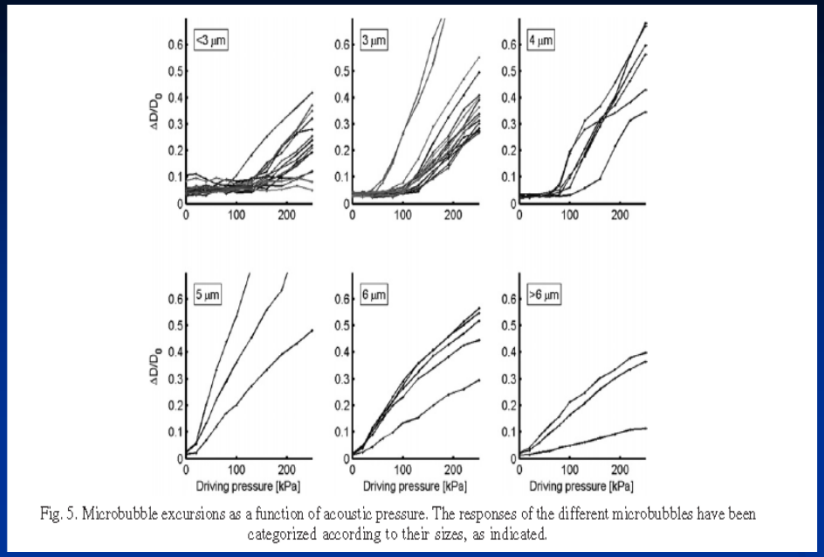

Fig. 5. Microbubble excursions as a function of acoustic pressure. The responses of the different microbubbles have been categorized according to their sizes, as indicated.

- Acoustic backscatter and attenuation experiments are employed in order to estimate shell elasticity and viscosity (van der Meer et al. JASA 2007, Sarkar et al. JASA 2005)
- Abrupt vibration onset (Emmer et al. Ultr. Med. Biol. 2007) - Reduction in resonance frequency with increasing sound amplitude, Overvelde et al. Ultr. Med. Biol. 2010

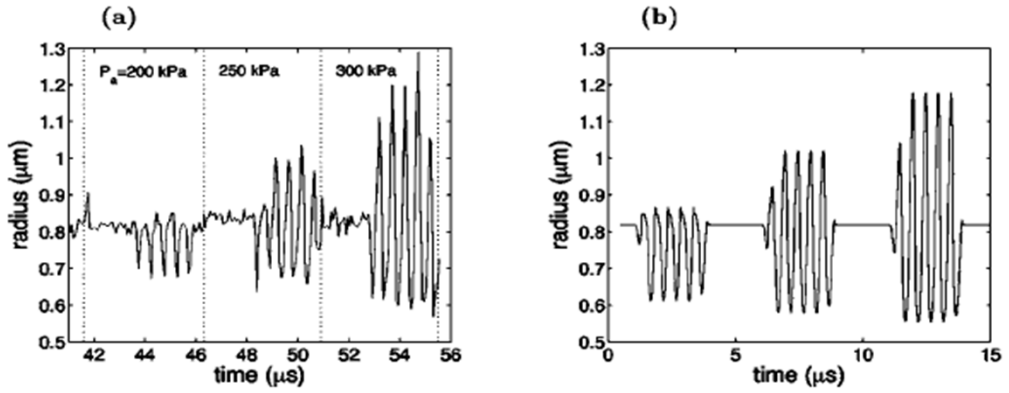

FIG. 8. (a) Experimental recordings of a BR14 bubble response to repeated 2 MHz pulses separated by 60 ms, with an increasing acoustic pressure. (b) Simulation with the same acoustic pressures. The fitted shell parameters are $R_{buckling}=R_0=0.82$ μm, $\chi=1$ N/m, $\kappa_s=7.2\times10^{-9}$ N, while the critical break-up is $\sigma_{break\text{-}up}=0.13$ N/m.

- Compression only behavior at low amplitudes followed by expansion only at large amplitudes, Marmottant et al. JASA 2005

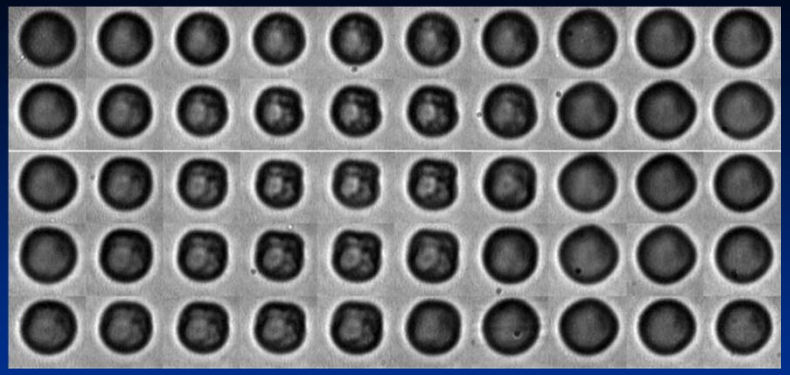

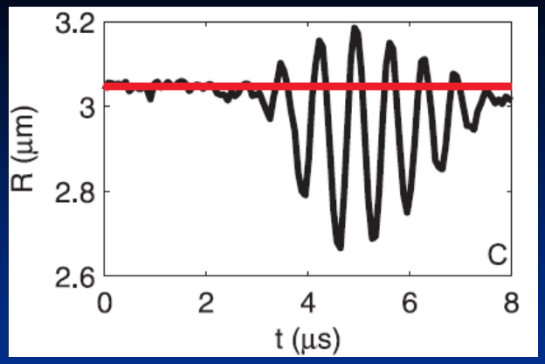

M. Overvelde,
Ph. D Thesis (2010)
Univ. Twente

$P_{Ac} = 40\text{kPa}, \quad \varepsilon = 0.4$

$BR - 14$

- **During compression only microbubble is only deformed during compression**

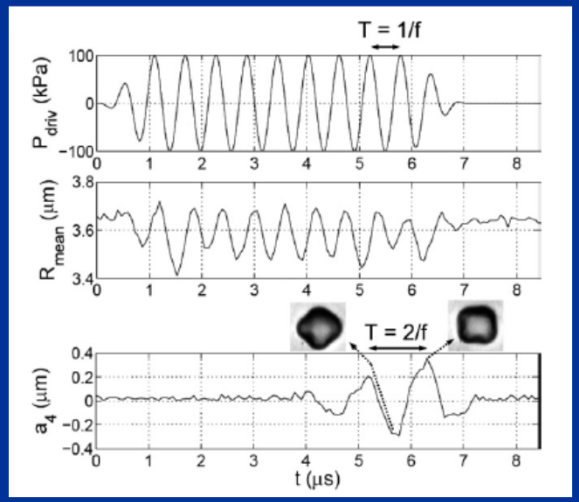

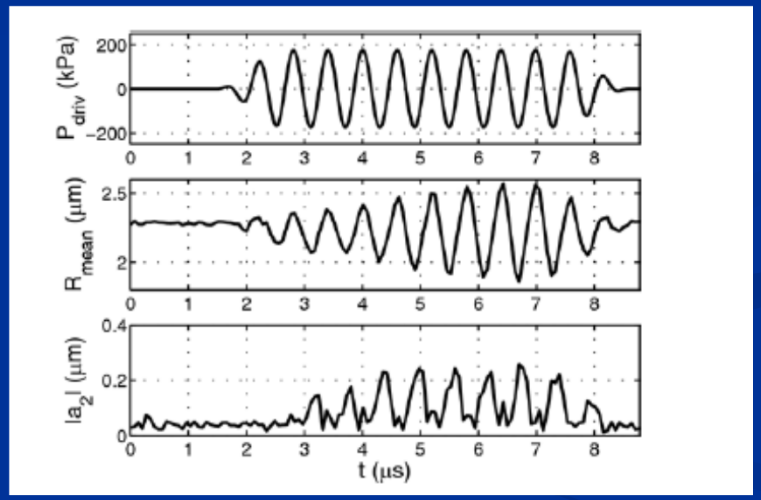

- Parametric shape mode excitation with or without compression only behavior (Dollet et. Al. Ultr. Med. Biol. 2008) – Harmonic and subharmonic shape mode excitation
- Rich harmonic content in the microbubble response (Paul et al. JASA 2010) is also useful in characterizing them – Sound amplitude threshold for radial and shape subharmonics provides possibility for parameter estimates

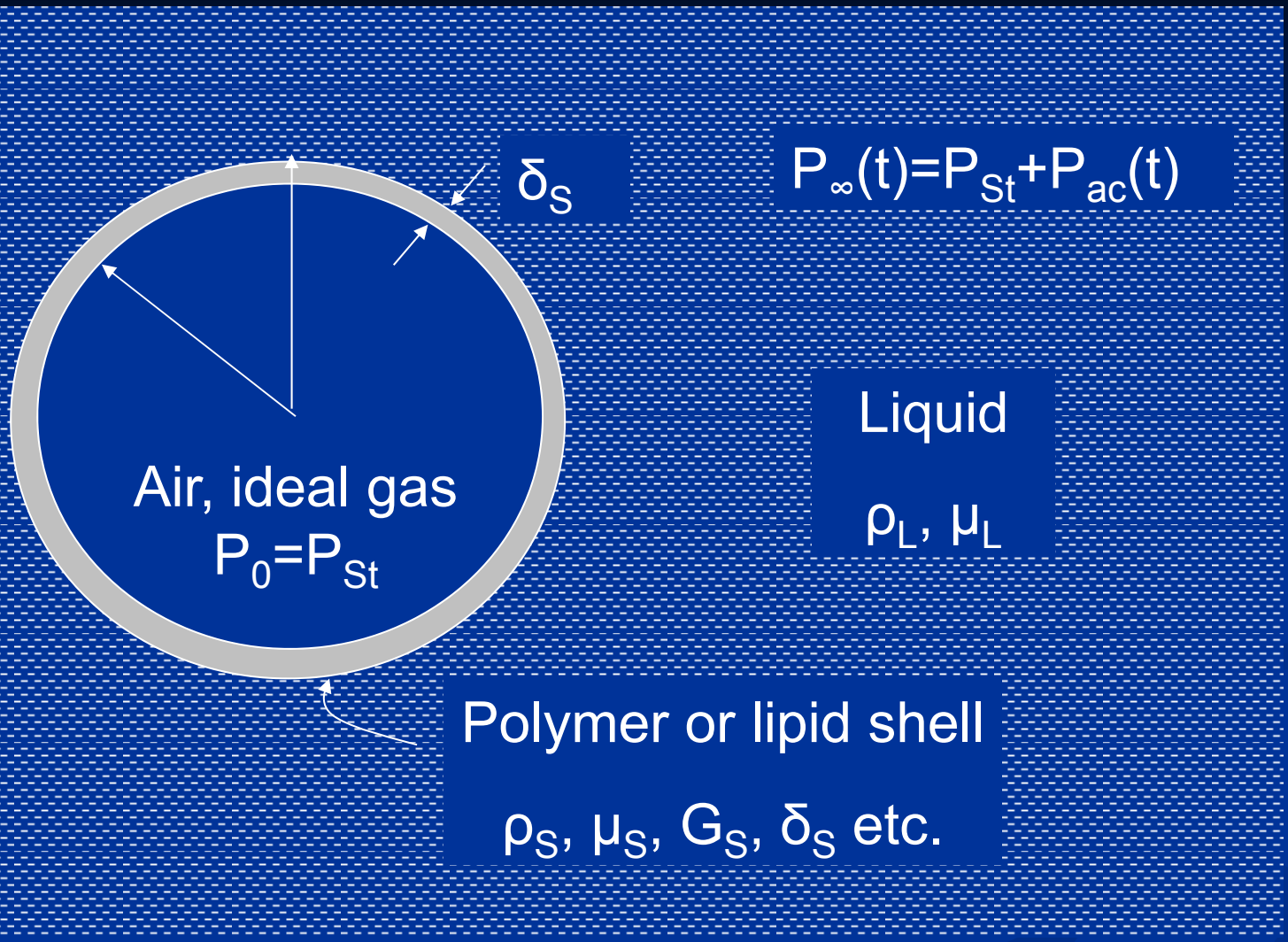

Schematic diagram of pulsating contrast agent

Available Models for the Shell

Viscoelastic solid

- Church: viscoelastic with constant G_S, μ_S, δ_S and negligible inertia
- de Jong: Linearized Church model
- Church-Hoff: Church model with negligible shell thickness to radius ratio
- Edwards viscoelastic model: Dilatational elasticity $E_S=3G_S$, dilatational viscosity μ_S, surface tension γ
- Marmottant et al model: Dilatational elasticity $E_S=3G_S$, dilatational viscosity μ_S, $R_{buckling}$
- Pelekasis & Tsigklifis: Viscoelastic solid model that accounts for nonlinear elastic effects (strain softening or strain hardening behavior) Bending elasticity, k_B, is added in order to capture deformation and break-up of shells
- Strain softening interfacial model (Sarkar et al.) : Viscoelastic solid model that accounts for nonlinear elastic effects (strain softening or strain hardening)

Viscoelastic liquid

- Doinikov & Dayton: Viscoelastic liquid model for lipid shells, relaxation time λS, dilatational viscosity, μS

- Hooke's law properly describes behavior of stiff polymeric shells
  Strain softening behavior captures most of the reported effects associated with phospholipid monolayers (except for compression only behavior) – Area density of lipid monolayers increases/decreases during compression/expansion and their stiffness increases/decreases as well
- Compression only is associated with shell deformation or bending and we postulate the reversible formation of bilayers as the mechanism for the effective strain hardening behavior of the shell that is manifested during compression only pulsations
- So when bending occurs and local curvature increases there is a sort of phase transition that occurs leading to formation of bilayers and switching to strain hardening behavior (lipid bilayers are strain hardening i.e. they become softer at compression due to less available contact area for the hydrophobic chains to interact)
- We would like to test this theory against the available experimental data from static and dynamic response of contrast agents
  Then we can estimate the appropriate parameters and achieve optimal design of new agents

Spherosymmetric Model

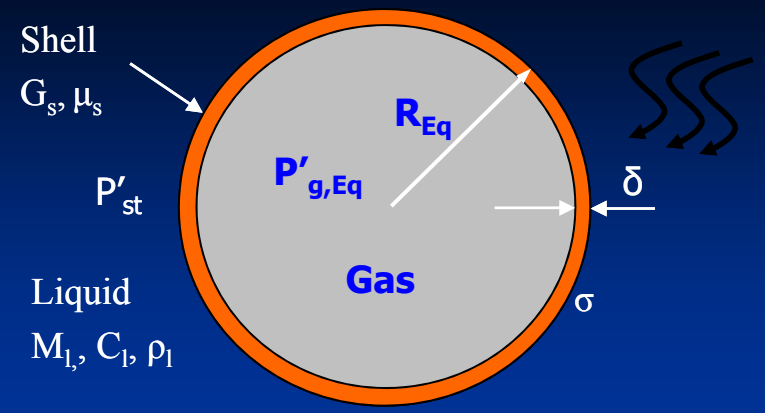

$$P'_{\infty}(t) = P'_{st}\left[1+\varepsilon\sin\left(\omega_f t'\right)\right] = P'_{St} + P'_{Ac}(t') \qquad \omega_f = 2\pi\nu_f$$

- Characteristic space and time scales: R_{Eq}, $1/\omega_f$
- Dimensionless parameters:

$$G = \frac{G_s\delta}{\rho\omega_f^2 R_{Eq}^3}, \quad P_{st} = \frac{P'_{St}}{\rho\omega_f^2 R_{Eq}^2}, \quad We = \frac{\rho R_{Eq}^3\omega_f^2}{\sigma}, \quad Re_l = \frac{\rho\omega_f R_{Eq}^2}{\mu_l},$$

$$Re_s = \frac{\rho\omega_f R_{Eq}^3}{\mu_s\delta}, \qquad M_l = \frac{\omega_f R_{Eq}}{C_l}$$

- Isothermal pulsations (γ~1)

$$P_g(t)V^{\gamma}(t) = P_{g,Eq}V_{Eq}^{\gamma}$$

- The Keller-Miksis model is used for the surrounding liquid

$$\left(1-M_l\dot{R}\right)R\ddot{R} + \left(\frac{3}{2} - \frac{M_l\dot{R}}{2}\right)\dot{R}^2 =$$

$$= \left(1+M_l\dot{R}\right)\left(P_l\big|_{r=R} - P_{st} - P_{Ac}\right) + M_l R\frac{d}{dt}\left(P_l\big|_{r=R} - P_{Ac}\right)$$

- Normal force balance on the shell-liquid interface relating jump in normal stress to the visco-elastic tensions on the shell

$$P_l\big|_{r=R} = \left(\frac{1}{R}\right)^{3\gamma}\left[P_{st} + \frac{2}{We} + \Delta F_{n,Eq}\right] + \\ -\frac{2}{WeR} - \frac{4\dot{R}}{Re_l R} - \Delta F_n$$

- Shell stress-strain constitutive law
  - **Kelvin-Voigt** law –Hooke's law with viscosity
  - **Mooney-Rivlin** law, strain-softening material
  - **Skalak** law, strain-hardening material

$$\Delta F_{n,MR} = 2\frac{G}{R}\left[1-\frac{1}{e^6}\right]\left[1+b\left(e^2-1\right)\right] + \frac{12}{Re_s}\frac{1}{eR}\frac{\partial e}{\partial t}$$

$$e = \frac{R}{1-u}$$

$$\Delta F_{n,SK} = 2\frac{G}{R}\left[(1-c)e^2 + ce^6 - 1\right] + \frac{12}{Re_s}\frac{1}{eR}\frac{\partial e}{\partial t}$$

Elastic Tensions

$$\underline{\underline{\tau}}_{El} = \frac{1}{J_S}\underline{\underline{A}}\cdot\frac{\partial w}{\partial \underline{\underline{e}}}\cdot\underline{\underline{A}}^T = \frac{2}{J_S}\left\{\frac{\partial w}{\partial I_1}\underline{\underline{A}}\cdot\underline{\underline{A}}^T + \frac{\partial w}{\partial I_2}J_S^2\left(\underline{\underline{I}} - \vec{n}\vec{n}\right)\right\},$$

$\underline{\underline{e}}$: Green-Lagrange deformation tensor

$$\underline{\underline{A}} = \left(\underline{\underline{I}} - \vec{n}\vec{n}\right)\cdot\frac{\partial \vec{x}}{\partial \vec{X}}\cdot\left(\underline{\underline{I}} - \vec{N}\vec{N}\right), \quad e = \frac{1}{2}\left[A^T\cdot A - (I - NN)\right]$$

$\underline{\underline{A}}$: Displacement gradient tensor

w: Elastic energy of the membrane

$\vec{X}, \vec{x}$: Reference and final position vectors of membrane particles

Principal extension ratios on a surface: $\lambda_i = \frac{ds_i}{dS_i}, i = 1,2, \quad e_i = \frac{1}{2}\left(\lambda_i^2 - 1\right)$

λ_i^2 : Eigenvalues of $\underline{\underline{A}}\cdot\underline{\underline{A}}^T$

$I_1 = \lambda_1^2 + \lambda_2^2 - 2, \quad I_2 = J_s^2 - 1 = \lambda_1^2\lambda_2^2 - 1$: Strain invariants

local elongation

local area dilation

$$\lambda_1 = \frac{\partial s/\partial\xi|_t}{\partial S/\partial\xi|_{Eq,t=0}}, \quad \lambda_2 = \frac{r\sin\theta|_t}{r\sin\theta|_{Eq,t=0}}:$$

Axisymmetry with unstressed initial configuration

$$\lambda_1 = \lambda_2 = \lambda = R(t)/R_{Eq}$$

Isotropic tension

Green & Zerna, Dover 2002, Barthes-Biesel et al., JFM 2002, Pozrikidis, CUP 1992

Shell Constitutive Laws-Isotropic Tension

- Linear behavior ⟶ Hooke's law
  Kelvin-Voigt law with viscous stresses

$$T_1^H = G_S \frac{1+\nu_s}{1-\nu_s}\left[\lambda^2 - 1\right] = K\left(\lambda^2 - 1\right) = K\frac{\Delta A}{A}$$

K: area dilatation modulus,
G_S: shear modulus

ΔA/A: relative area change

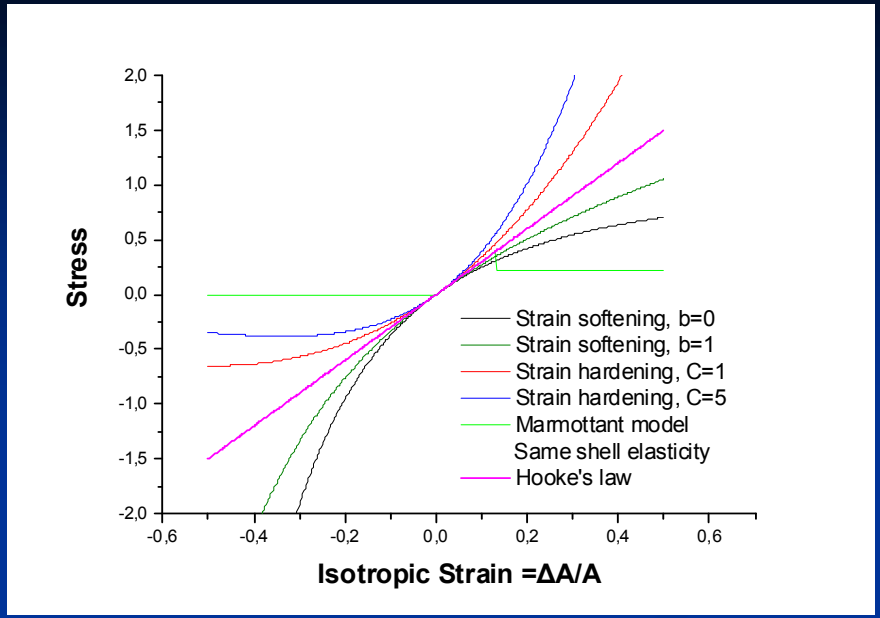

- Strain softening material (e.g. rubber like material) ⟶ 2D Mooney-Rivlin law

$$T_1^{MR} = \frac{G_{MR}\left(\lambda^4 + \lambda^2 + 1\right)}{\lambda^6}\left[\lambda^2 - 1\right]\left[\Psi + \lambda^2\left(1 - \Psi\right)\right], \quad 0 \le \Psi \le 1$$

Ψ=1-b: degree of smoothness, unlimited area dilatation

- Strain hardening material (e.g. red blood-cell membrane) ⟶ Skalak law

$$T_1^{SK} = G_{SK}\left[\lambda^2 - 1\right]\left[1 + C\lambda^2\left(1 + \lambda^2\right)\right], \quad 1 \le C,$$

C: degree of area compressibility

In the limit of small deformations, $||e_i||<<1$, all hyperelastic laws reduce to Hooke's law

$$MR: G_{MR} \to G_S \text{ when } \nu_S = 1/2, \quad SK: G_{SK} \to G_S \text{ when } \nu_S = C/(1+C),$$

Viscous Tensions

$$\underline{\underline{\tau}}_{vis} = 2\mu_{Sh}\underline{\underline{\dot{\gamma}}} + \left(\kappa_{Dil} - \mu_{Sh}\right)\left(\underline{\underline{I}} : \underline{\underline{\dot{\gamma}}}\right)\underline{\underline{I}}$$

Interfacial transport processes and rheology, Edwards et al., 1991

μ_{Sh} : *shear viscosity* κ_{Dil} : *dilatational viscosity*

In the absence of rheological data $\kappa_{Dil}=\mu_{Sh}$

$\underline{\underline{\dot{\gamma}}}$: rate of strain per unit deformed surface, $\dot{\gamma}_1 = \frac{1}{\lambda_1}\frac{\partial \lambda_1}{\partial t}$

- We can have shear thinning or shear thickening effects, e.g. the Cross-Carreau model

$$\mu_s\left(\dot{\gamma}_{ij}\right) = \mu_\infty + \left(\mu_0 - \mu_\infty\right)\left[1 + \left(k\dot{\gamma}_{ij}\right)^\alpha\right]^{\frac{n-1}{\alpha}}, \quad \alpha = 2 = 1 - n$$

μ_∞ : viscosity at infinite shear, μ_0 : viscosity at zero shear, k: time constant

Isotropic Tension

$\underline{\underline{\tau}}_{surf} = \sigma\underline{\underline{I}}$, σ : *surface tension*

Interfacial Force Balance

$$\left[\underline{\underline{\tau}} \cdot \vec{n}\right] \equiv \underline{\underline{\tau}}_{liq} \cdot \vec{n} - \underline{\underline{\tau}}_{gas} \cdot \vec{n} = \vec{\nabla}_s \cdot \left(\underline{\underline{\tau}}_{El} + \underline{\underline{\tau}}_{vis} + \underline{\underline{\tau}}_{sur}\right)$$

Radial Pulsations - Effect of sound amplitude

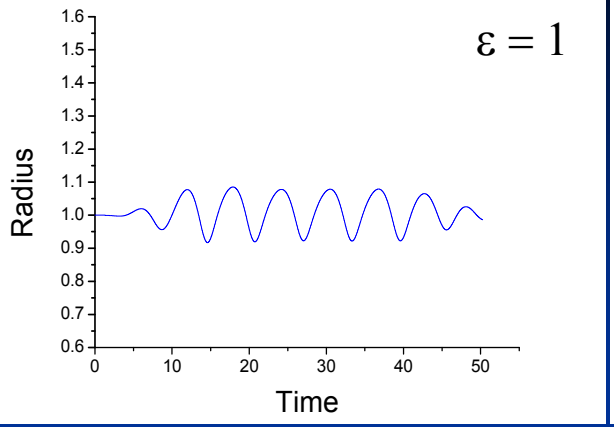

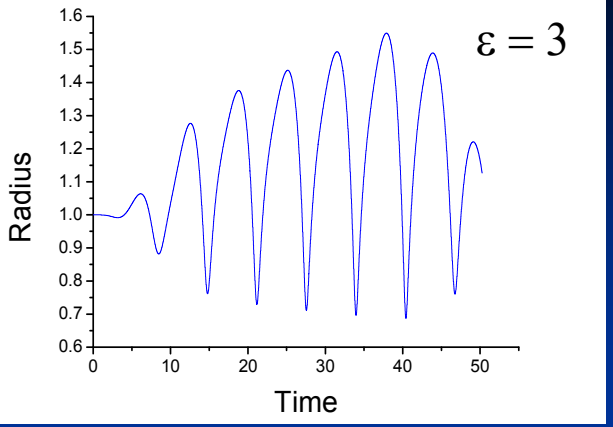

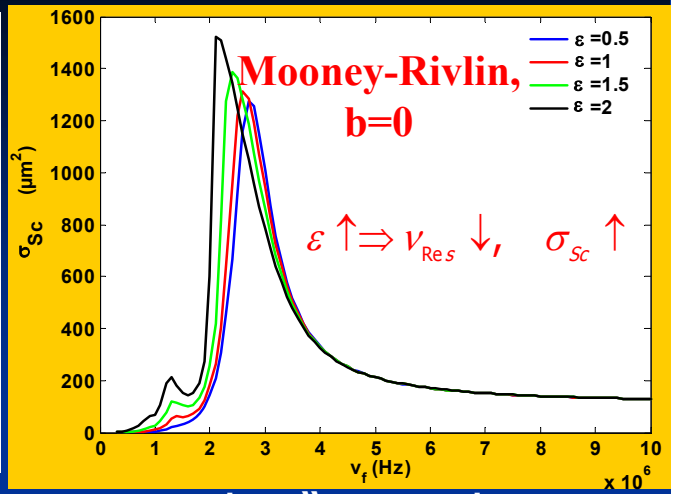

Strain softening shells (e.g. lipid monolayers prefer to be at expansion "expansion only behavior" – Their resonance frequency decreases with sound amplitude

- Estimation of Gs, μc, in the standard fashion in the small amplitude regime

ρ_l=998 kg/m^3, σ=0.045 kg/s^2, R =3*10^{-6} m, G_s=35 MPa, μ_S=0.6 kg m^{-1}s^{-1}, δ=15 nm

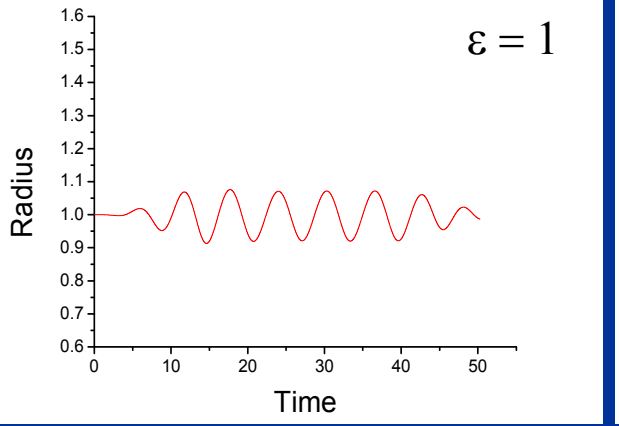

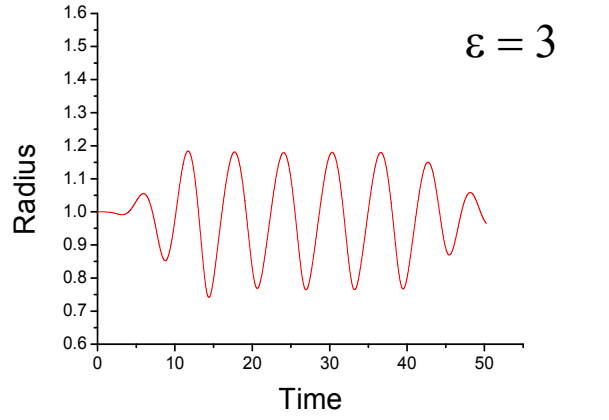

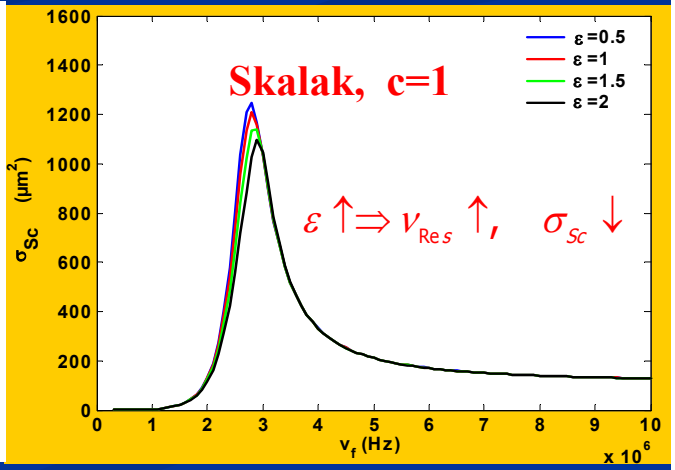

Strain hardening shells (e.g. lipid bilayers prefer to be at compression "compression only behavior" – Their resonance frequency increases with sound amplitude

Abrupt vibration onset

C_l=1500 m/s, P_{st}=101325 Pa, γ=1.4, ρ_l=998 kg/m^3, σ=0.045 kg/s^2, ν_f=1.7 MHz

μ_l=0.001 kg m^{-1}s^{-1}, μ_S=0.6 kg m^{-1}s^{-1}, G_S=35 MPa, δ=15 nm, u=0, BR14

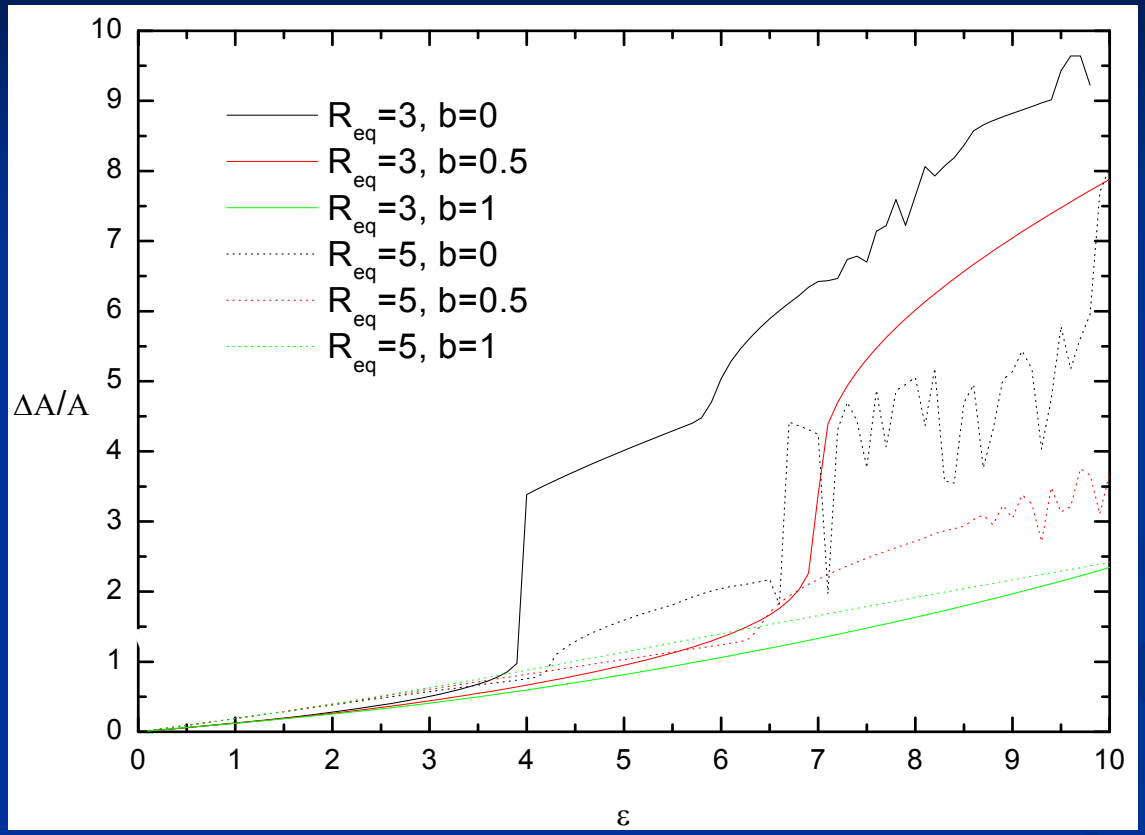

Tsiglifis & Pelekasis, JASA 2008

- Estimation of parameter b via high amplitude acoustic measurements
- Abrupt vibration onset is due to the decrease in the resonance frequency with increasing amplitude (for small bubbles)-softer bubbles exhibit a more abrupt vibration onset
- Large bubbles never exhibit an abrupt vibration onset since their resonance frequency is already smaller than the forcing frequency at small amplitudes

Comparison with experimental measurements (Sarkar et al.)

C_l=1500 m/s, P_{st}=101325 Pa, γ=1.4, ρ_l=998 kg/m^3, R_{eq} =1.6*10^{-6} m, μ_l=0.001 kg m^{-1}s^{-1}, G_s=52 MPa, μ_S=0.99 kg m^{-1}s^{-1}, δ=4 nm (**Sonazoid**)

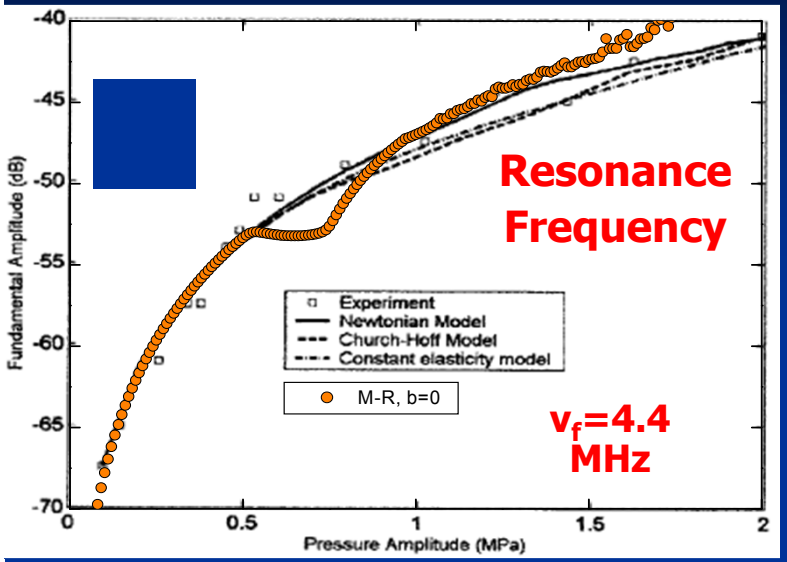

Shell viscosity is estimated from measurements on resonance

Shell viscosity is decreased due to shear thinning effect

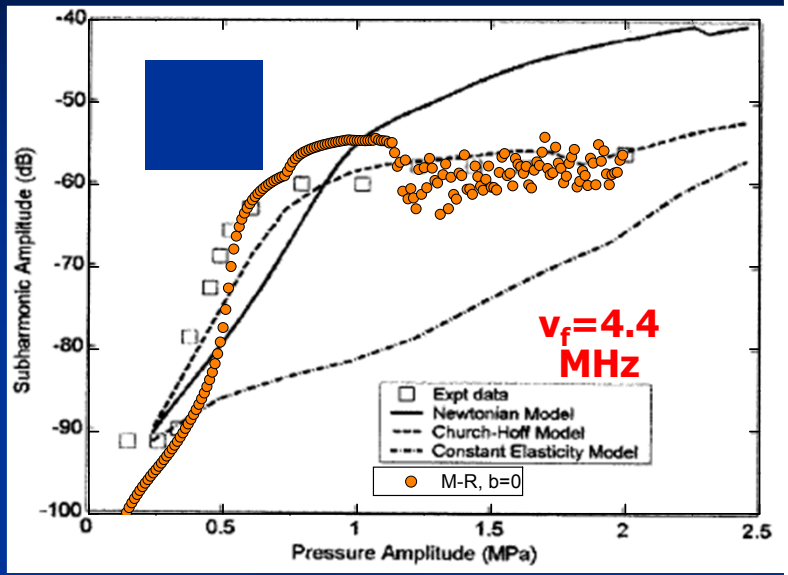

$$\mu_{Sh} \sim \dot{\gamma}^{n-1} \sim \omega^{n-1} \xrightarrow{n<1} \omega \downarrow \rightarrow \mu_{Sh} \uparrow$$

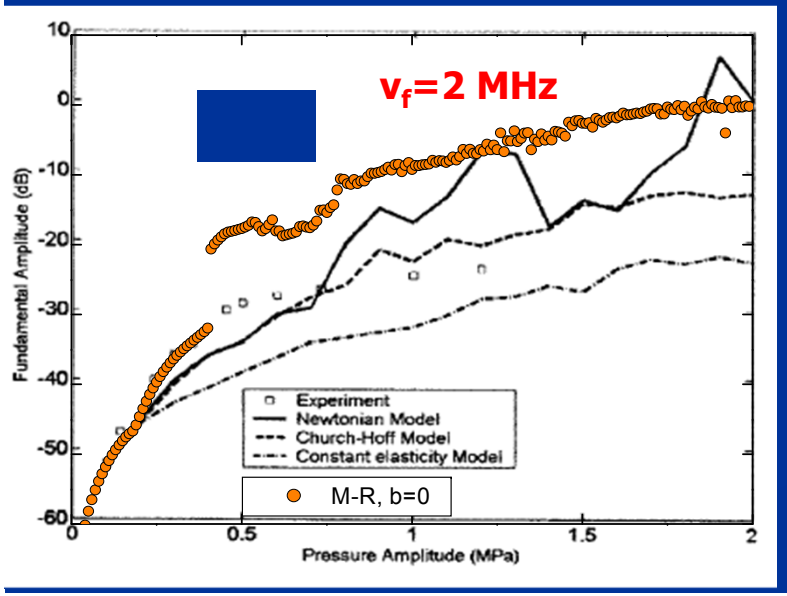

At lower frequencies viscosity increases and scattering effect is overestimated

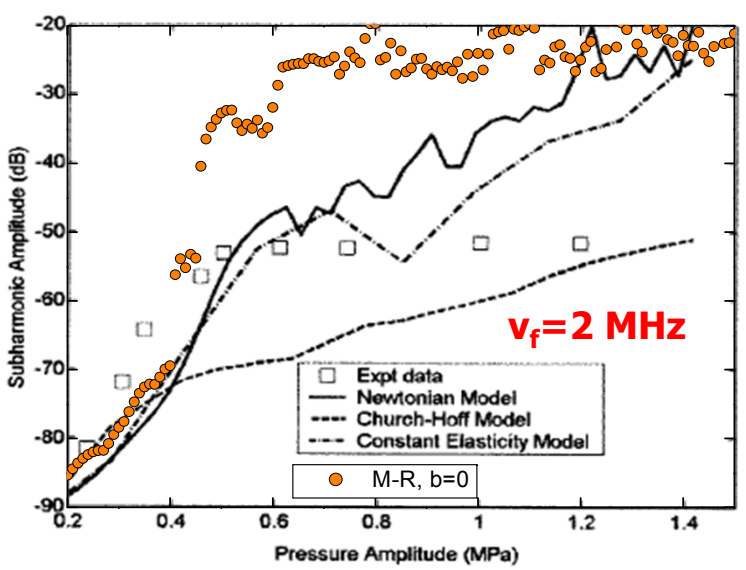

Axisymmetric Pulsations

$$P'_{\infty}(t') = P'_{st}\left[1+\varepsilon\cos\left(\omega_f t'\right)\right], \quad \omega_f = 2\pi\nu_f$$

$G_{S,2d}=\delta G_S$

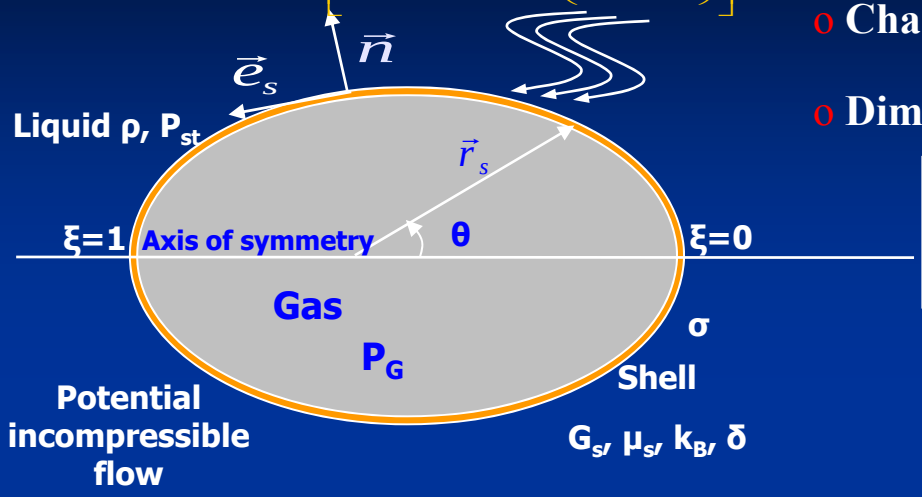

- Characteristic space and time scales: $R_{Eq}, \sqrt{\rho R_{Eq}^3 / G_{S,2}}$
- Dimensionless parameters:

$$\omega_f = \frac{\omega'_f}{\sqrt{G_{S,2d}/\left(\rho R_{Eq}^3\right)}} \qquad P = \frac{P_{St} R_{Eq}}{G_{S,2d}}, \qquad We = \frac{G_{S,2d}}{\sigma}$$

$$\mathrm{Re}_l = \sqrt{\frac{\rho G_{S,2d} R_{Eq}}{\mu_l^2}} \qquad B = \frac{k_B}{G_{S,2d} R_{Eq}^2} \qquad \mathrm{Re}_s = \sqrt{\frac{\rho G_{S,2d} R_{Eq}^3}{\mu_S^2}}$$

- Axisymmetry
- Ideal, irrotational flow
- Incompressible surrounding fluid with a sinusoidal pressure change in the far field
- Ideal gas in the microbbule undergoing isothermal pulsations
- Very thin viscoelastic shell, often a phospho-lipid monolayer, whose behavior is characterized by the constitutive law, e.g. Hookes's, Mooney-Rivlin or Skalak law
- The shell may be pre-stressed but is always at equilibrium
- The shell parameters are: area dilatation modulus, $\chi=3G_S\delta$, dilatational viscosity, μ_S, degree of softness or area compressibility, b or C for strain softening or strain hardening shells, and the bending modulus, k_B

Formulation

- Potential incompressible flow $\vec{u} = \vec{\nabla}\Phi, \quad \nabla^2\Phi = 0$
- **Boundary integral equation for the Laplacian**

$$-\Phi(\theta',t) + \int_0^N \left[\Phi(\theta,t) - \Phi(\theta',t)\right] \frac{\partial G}{\partial n}(r,r',\theta,\theta') r \left(r_\xi^2 + \left(r\theta_\xi\right)^2\right)^{1/2} \sin\theta d\xi =$$

$$\int_0^N \frac{\partial \Phi}{\partial n}(\theta,t) G(r,r',\theta,\theta') r \left(r_\xi^2 + \left(r\theta_\xi\right)^2\right)^{1/2} \sin\theta d\xi$$

- **Radial part of the Kinematic condition for interfacial particles** $\vec{u}\cdot\vec{e}_r = \vec{\nabla}\Phi\cdot\vec{e}_r = \frac{d\vec{r}_s}{dt}\cdot\vec{e}_r$
- **Isothermal pulsations inside the shell** $PV^\gamma = P_0 V_0^\gamma, \quad \gamma = 1.07$
- Force balance on the interface

$$\vec{r} = \vec{r}_s : \left(-P_L \underline{\underline{I}} + \frac{1}{\mathrm{Re}_L}\underline{\underline{X}}\right)\cdot\vec{n} + P_G\vec{n} = \frac{2k_m}{We}\vec{n} + \overrightarrow{\Delta F} = \frac{\left(\vec{\nabla}_s\cdot\vec{n}\right)\vec{n}}{We} + \overrightarrow{\Delta F},$$

$$\overrightarrow{\Delta F} = \Delta F_n\vec{n} + \Delta F_t\vec{e}_s = -\vec{\nabla}_s\cdot\underline{\underline{T}}, \quad \underline{\underline{T}} = \underline{\underline{\tau}}_{El} + \vec{e}_s\vec{q} + \underline{\underline{\tau}}_{Vis}$$

$\vec{\nabla}_s$: **Surface gradient** $\underline{\underline{T}}$: **Stress tensor**

$\underline{\underline{\tau}}_{El}$, $\underline{\underline{\tau}}_{vis}$: **Elastic and viscous stress tensors**

$\vec{q}\vec{n}$: **Transverse shear tensor due to bending moments**

- **Dynamic boundary condition**

Via Bernoulli's law in the liquid

$$\frac{D\Phi}{Dt} = \frac{1}{2}\left[\left(\frac{\partial\Phi}{\partial n}\right)^2 + \frac{\Phi_\xi^2}{r_\xi^2 + r^2\theta_\xi^2}\right] + P_\infty - P_G + \frac{2k_m}{We} + \Delta F_n$$

- Torque balance on the interface

$$\vec{q} = \vec{\nabla}_s \cdot \underline{\underline{m}} \cdot (\underline{\underline{I}} - \vec{n}\vec{n}), \qquad \underline{\underline{m}} : \text{tensor of bending moments}$$

$$\underline{\underline{m}} = k_B\left(I_1, I_2, k_m\right) \cdot \left[\vec{\nabla}_s \vec{n} - k_m^R (\underline{\underline{I}} - \vec{n}\vec{n})\right]$$

Constitutive law for bending moments for axisymmetry and small deviations from the reference curvature

k_m^R : **Mean reference curvature** k_B : **Bending resistance** ν : **Poisson's ratio**

$$m_s = \frac{k_B}{\lambda_\varphi}\left(K_s + \nu K_\varphi\right), m_\varphi = \frac{k_B}{\lambda_s}\left(K_\varphi + \nu K_s\right) \qquad K_s \equiv \lambda_s k_s - k_s^R, K_\varphi \equiv \lambda_\varphi k_\varphi - k_\varphi^R$$

Bending measures of strain, Zarda et al. 1977
Following the theory of plates, and shells

$$k_B = \frac{3G_s\delta^2}{12\left(1-\nu^2\right)},$$ 3d elastic solid of small thickness h, Timoshenko & Krieger 1959

- For a molecular membrane whose bending moments depend on the solid angles subtended by molecular networks,
- k_B is viewed as bending elasticity, distinct from membrane elasticity, G_S, due to the anisotropy of the thin shell

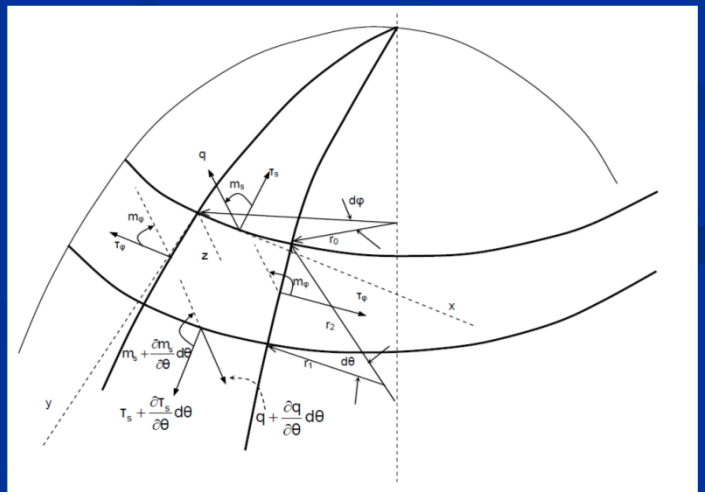

- Shell viscosity dominates liquid viscosity, $Re_s << Re_l$ and we can drop viscous stresses on the liquid side.
- Therefore the tangential force balance is satisfied on the shell with the viscous and elastic stresses in the shell balancing each other.
- Consequently this is a uniform approximation and does not require the introduction of a boundary layer in the liquid side

- **Linear stability analysis is performed on radially pulsating microbubbles, in order to identify**
  - ♦ **Critical pressure load for static buckling**
  - ♦ **Eigenfrequencies of axisymmetric shape modes of coated microbubbles**
  - ♦ **Phase diagrams, i.e. amplitude threshold of the acoustic disturbance, as a function of bubble radius for fixed forsing frequency, for parametric shape mode excitation and dynamic buckling**
  - ♦ **Effect of pre-stress on the above thresholds**
- **Numerical simulation of axisymmetric pulsations in order to identify**
  - ♦ **Nonlinear response with large deformations from sphericity**
  - ♦ **Threshold between steady pulsations and transient break-up**
  - ♦ **Dynamic route to compression only behavior**

Axisymmetric Stability

$r_d = R(t) + \delta w(\theta,t) + O(\delta^2)$ $\quad w(\theta,t)$: **Radial displacement of the interface**

$\theta_d = \theta + \delta \dfrac{u(\theta,t)}{R(t)} + O(\delta^2), \ \delta \ll 1$ $\quad u(\theta,t)$: **Angular displacement of the interface**

$$\vec{V} = \vec{V}^0 + \delta\vec{V}^1 + O(\delta^2), \quad P = P^0 + \delta P^1 + O(\delta^2), \quad P_G = P_G{}^0 + \delta P_G{}^1 + O(\delta^2), \quad \Phi = \Phi^0 + \delta\Phi^1 + O(\delta^2)$$

$$\Delta F_N = \Delta F_N^0 + \delta\Delta F_N^1 + O(\delta^2), \quad \Delta F_t = \Delta F_t^0 + \delta\Delta F_t^1 + O(\delta^2)$$

O(δ⁰) ⟶

$$R\ddot{R} + \frac{3}{2}\dot{R}^2 = P_G(t) - \frac{2k_m^0}{We} - \Delta F_N^0 - P_\infty(t), \ R(t=0) = R_{Eq}, \dot{R}(t=0) = 0$$

O(δ) $\quad \underline{\underline{A}} \cdot \begin{Bmatrix} \alpha_n \\ \beta_n \end{Bmatrix} = \begin{Bmatrix} 0 \\ 0 \end{Bmatrix}$ ⟶

$$\ddot{w}_n + \frac{3\dot{R}}{R}\dot{w}_n + \left[\frac{(1-n)\ddot{R}}{R} + \frac{(n+1)(n-1)(n+2)}{WeR^3}\right] w_n +$$

$$+ \frac{n+1}{R}\Delta F_N^1(\dot{w}_n, \dot{\psi}_n, w_n, \psi_n, B, \nu, \mathrm{Re}_s, R, \dot{R}, n) = 0$$

$$\Delta F_t^1(\dot{w}_n, \dot{\psi}_n, w_n, \psi_n, B, \nu, \mathrm{Re}_s, R, \dot{R}, n) = 0$$

$w_n(t) = \alpha_n e^{\omega_n t}$,

$\psi_n(t) = \beta_n e^{\omega_n t}$ $\quad u = \dfrac{\partial\psi}{\partial\theta}$

$R = 1, \ \dot{R} = \ddot{R} = 0$

Eigenfrequencies for shape pulsations

$$\det \underline{\underline{A}}\left[\omega_n; B, \nu, \mathrm{Re}_s, We, n\right] = 0$$

$\dot{R} = \ddot{R} = 0$

Criteria for static buckling

$$\det \underline{\underline{A}}\left[\omega_n; R(P_{Cr}), B, \nu, \mathrm{Re}_s, n\right] = 0$$

P_{Cr}: minimum external overpressure for $\mathrm{Re}(\omega_n)$ to cross zero for some n

Stability of Periodic Solutions (Floquet analysis)

$\ddot{R}, \dot{R}, R, \quad period\ T = \frac{2\pi}{\omega_f}$ ⟶ **Known from the solution of the O(δ^0) problem**

⟶

$$\frac{d}{dt}\begin{pmatrix} y_1 \equiv w_n \\ y_2 \equiv \dot{w}_n \\ y_3 \equiv \psi_n \end{pmatrix} = \begin{pmatrix} f_1 \\ f_2 \\ f_3 \end{pmatrix} = \begin{pmatrix} y_2 \\ -\left\{ 3\frac{\dot{R}}{R} y_2 + \left[\frac{(1-n)\ddot{R}}{R} + \frac{(n+1)(n-1)(n+2)}{We R^3} \right] y_1 + \right. \\ \left. + \frac{n+1}{R} \Delta F_n^1 \left(y_1, y_2, y_3, Q, R, \dot{R} \right) \right\} \\ Q\left(y_1, y_2, y_3, R, \dot{R} \right) \end{pmatrix}$$

$$\begin{pmatrix} \vec{y}(\tau=0) - \vec{y}(\tau=1) \\ f_k\left(\vec{y}(\tau=0); \tau=0\right) \end{pmatrix} = 0$$

Stability is determined by the eigenvalues μ_j of the Monodromy materix M:

$$\underline{\underline{M}} = \underline{\underline{\Phi}}(T), \qquad \dot{\underline{\underline{\Phi}}} = \frac{\partial \vec{f}}{\partial \vec{y}} \cdot \underline{\underline{\Phi}}, \qquad \underline{\underline{\Phi}}(0) = \underline{\underline{I}}$$

$\vec{y}(t)$ is stable *when* $|\mu_j| < 1$ *for* $j = 1, \ldots\ldots, n-1$

$\vec{y}(t)$ is unstable and $2T$ *periodic when* $\mathrm{Im}(\mu_j) = 0$ *and* $\mathrm{Re}(\mu_j) < -1$ (subharmonic resonance)

$\vec{y}(t)$ is unstable and T *periodic when* $\mathrm{Im}(\mu_j) = 0$ *and* $\mathrm{Re}(\mu_j) > 1$ (harmonic resonance)

$\vec{y}(t)$ is unstable but not periodic when $\mathrm{Im}(\mu_j) \neq 0$ *and* $|\mu_j| > 1$ (bifurcation into a torus)

Numerical Methodology

Algorithm

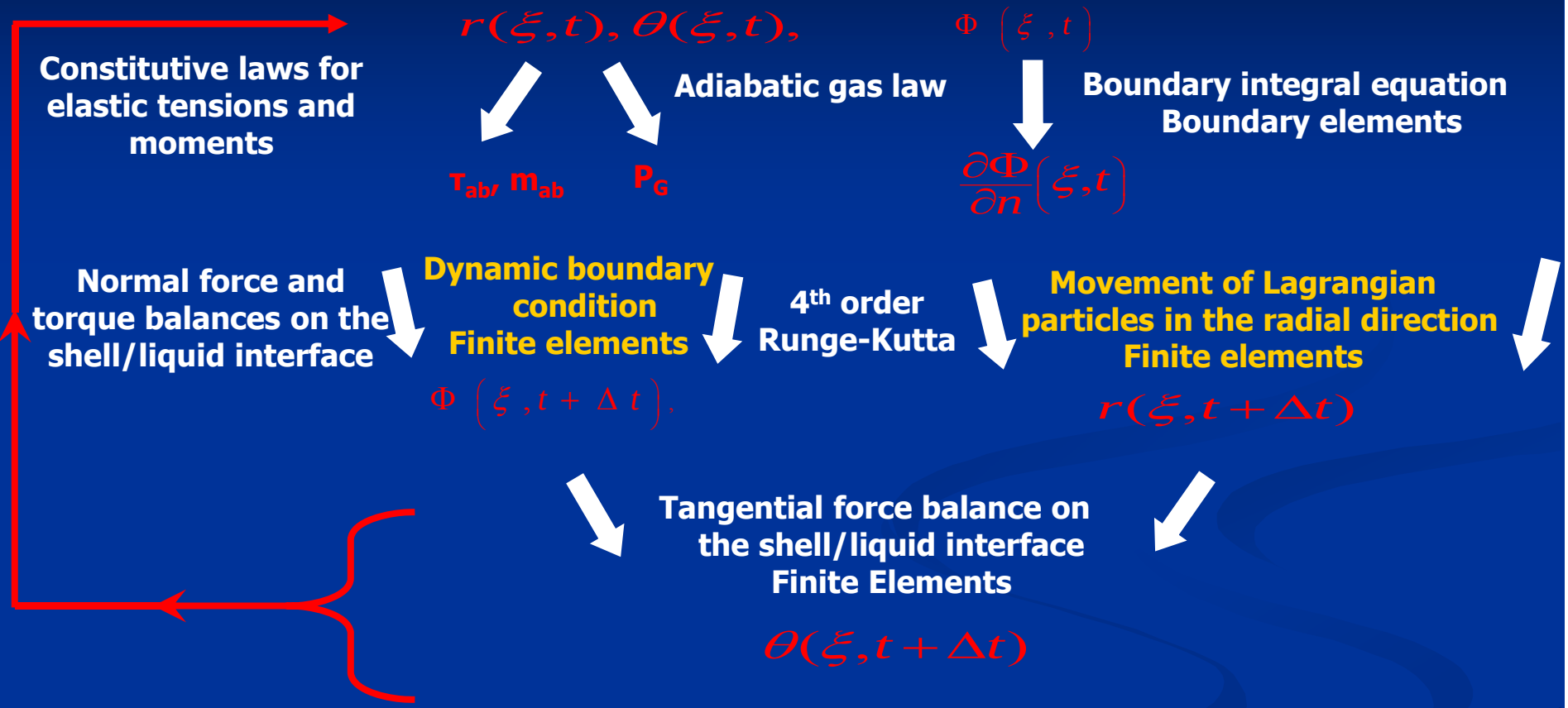

Linear Stability Analysis Results

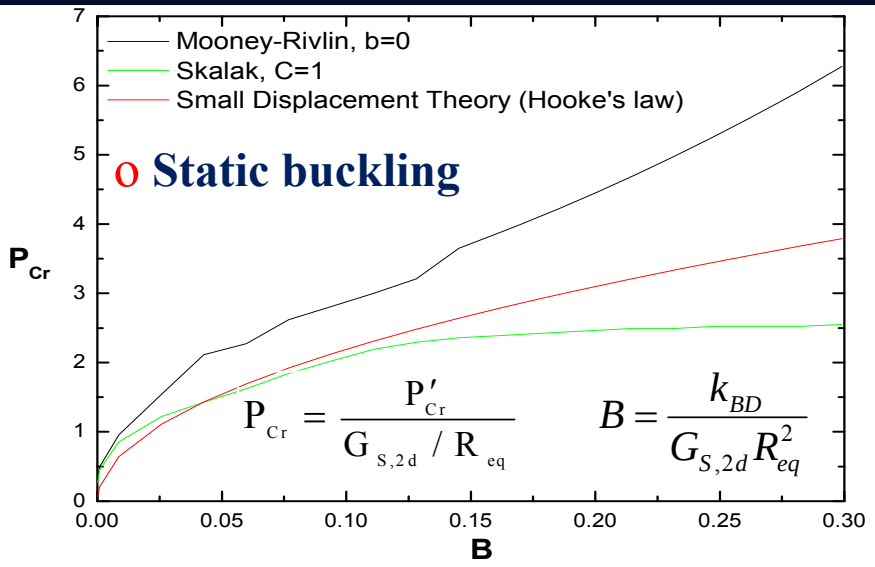

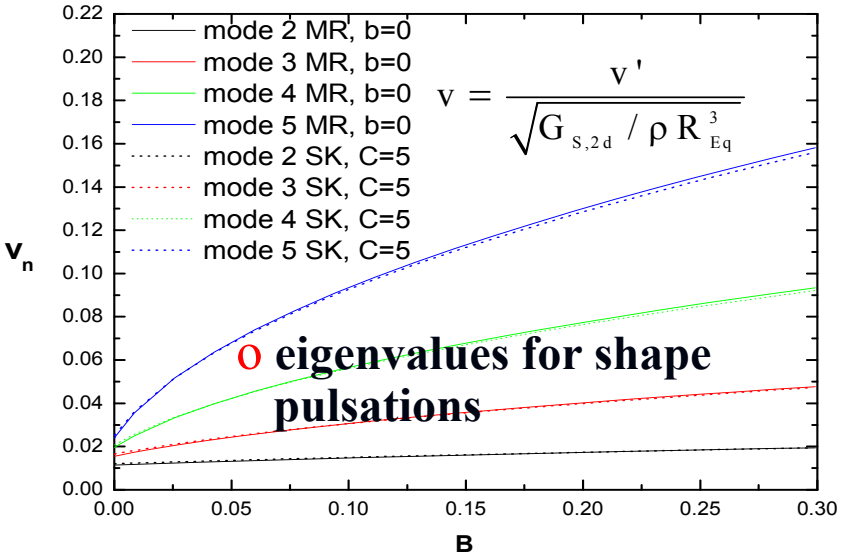

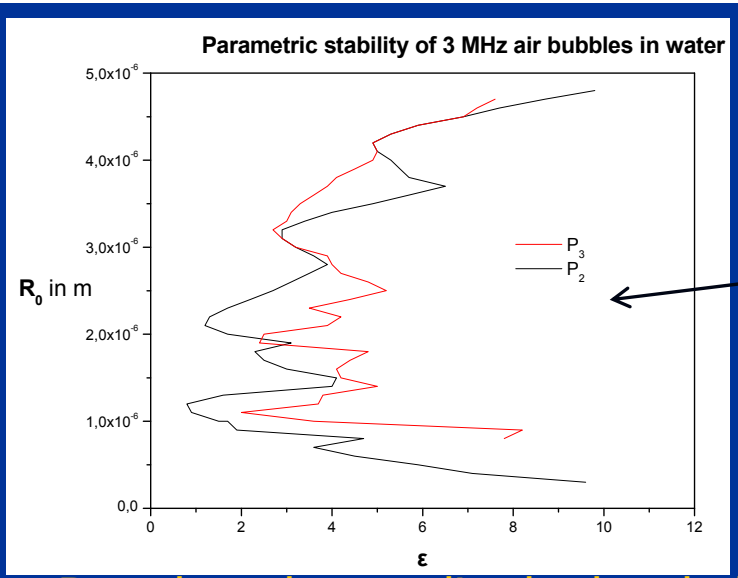

Phase Diagrams

Gas Bubbles

BR14

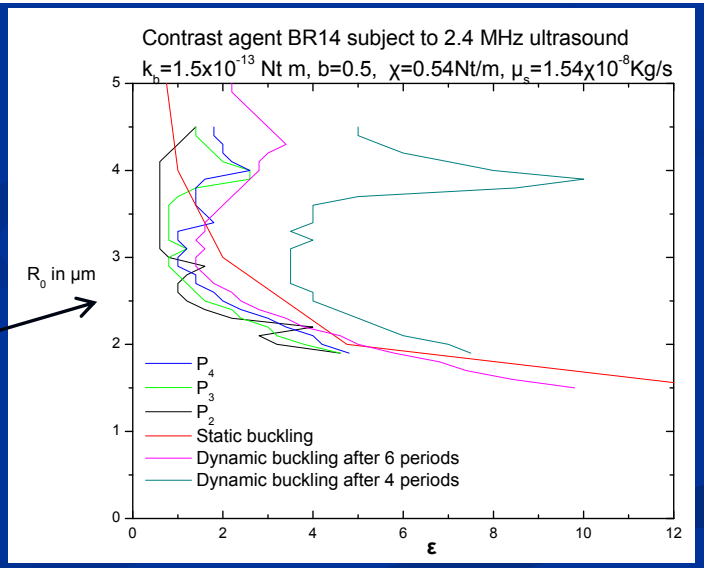

- Based on the amplitude thresholds for shape deformation k_b can be estimated
- Separation between threshold curves corresponding to parametric excitation of successive modes is smaller in comparison with phase diagrams of free bubbles

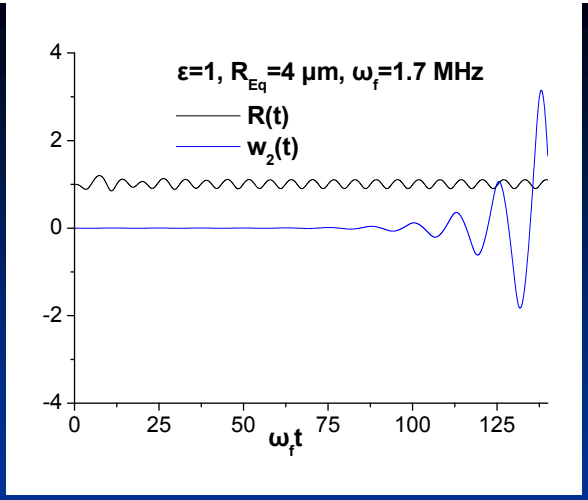

- Subharmonic excitation of shape modes beyond a certain amplitude threshold

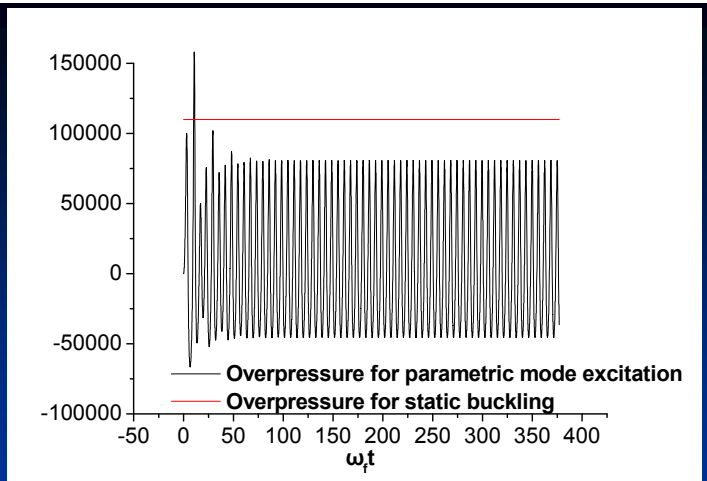

Occurs gradually over a number of periods of the acoustic excitation

Dynamic overpressure below threshold for static buckling

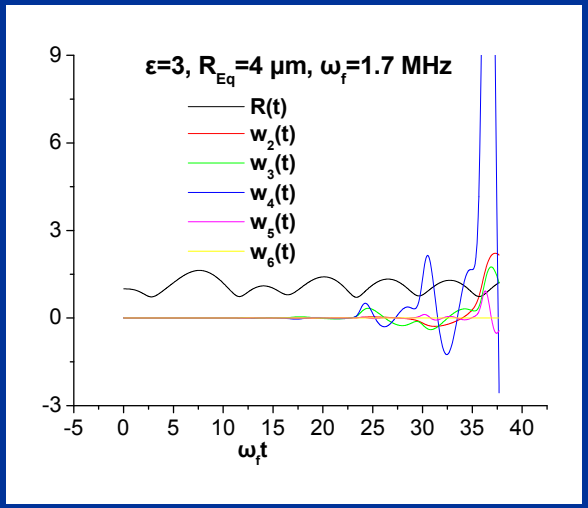

- Explosive excitation of shape modes beyond a different threshold amplitude:
- Dynamic buckling – equivalent to Rayleigh-Taylor nstability for free bubbles

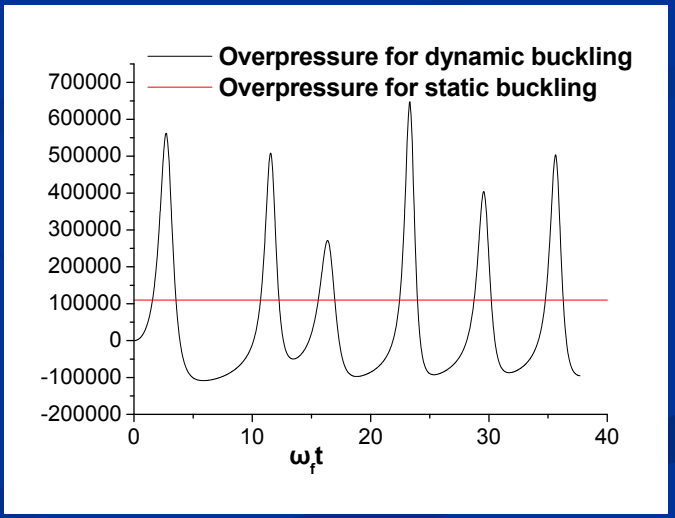

Dynamic overpressure above threshold for static buckling

Tsigklifis & Pelekasis, Physics of Fluids 2011

Static Buckling Instability

R_0=1.0 μm, μ_s=7 Pa*s, G_{3D}=88 MPa, k_B=3.616d-16 N*m, ε=2.0,
b=0, γ=1.07, ν=0.5, Pst=101325Pa, μ_i=0, h=23.1 nm

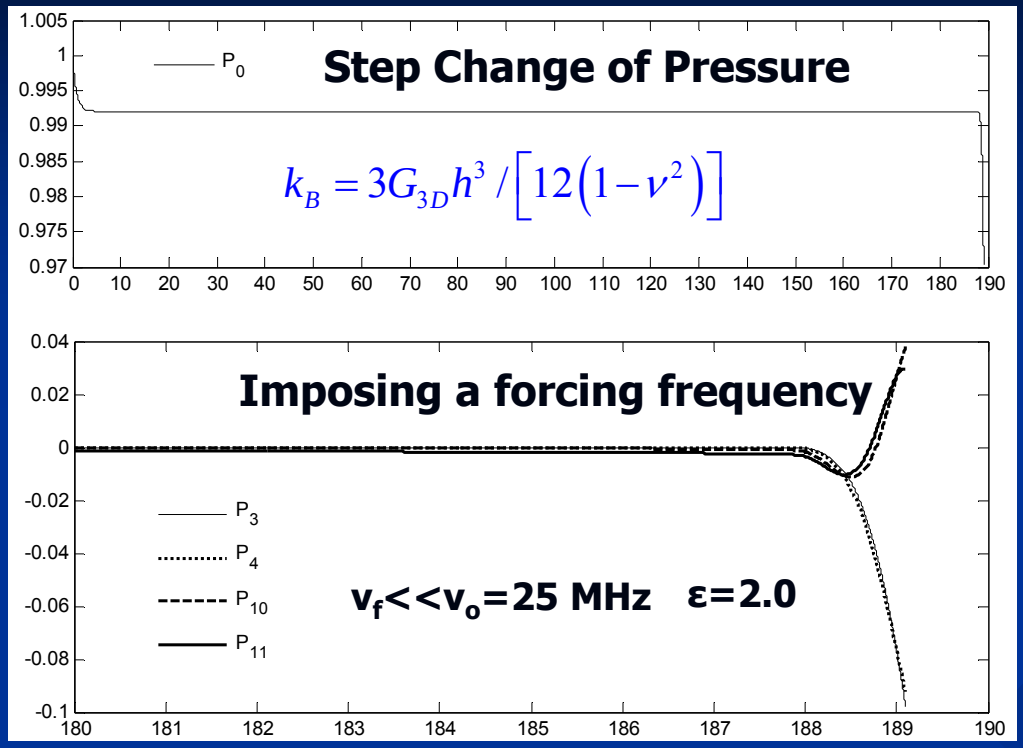

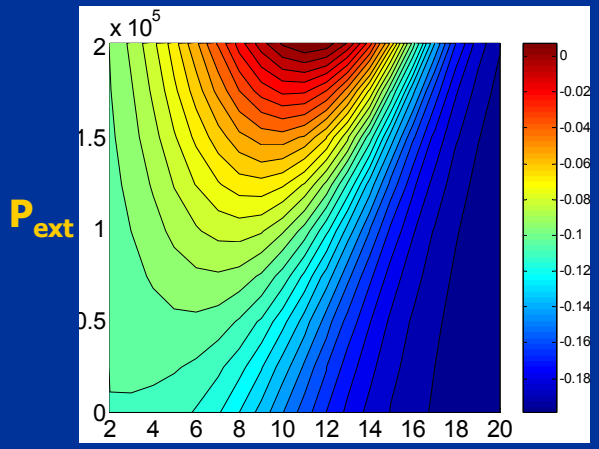

- Static stability and dynamic simulations provide same amplitude threshold and eigenmode

Contrast agent PB127
polymer/albumin shell

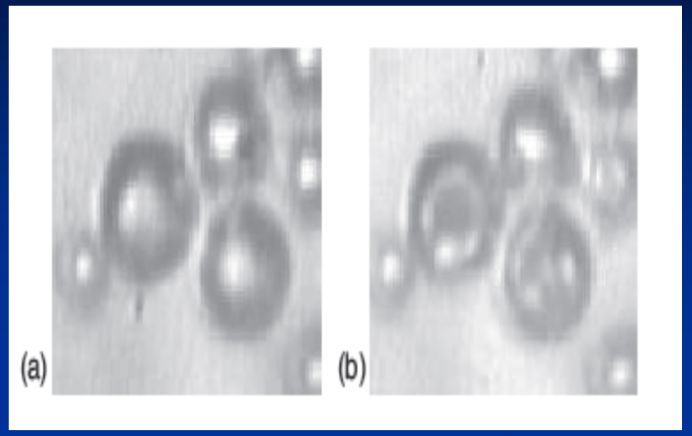

Bouakaz et al.(2011) (2005) optical observations

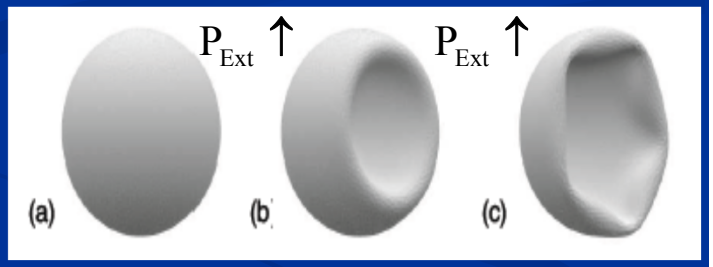

P. Marmottant et al.(2011) with surface evolver

Dynamic Stability and Simulations of Polymeric Shells

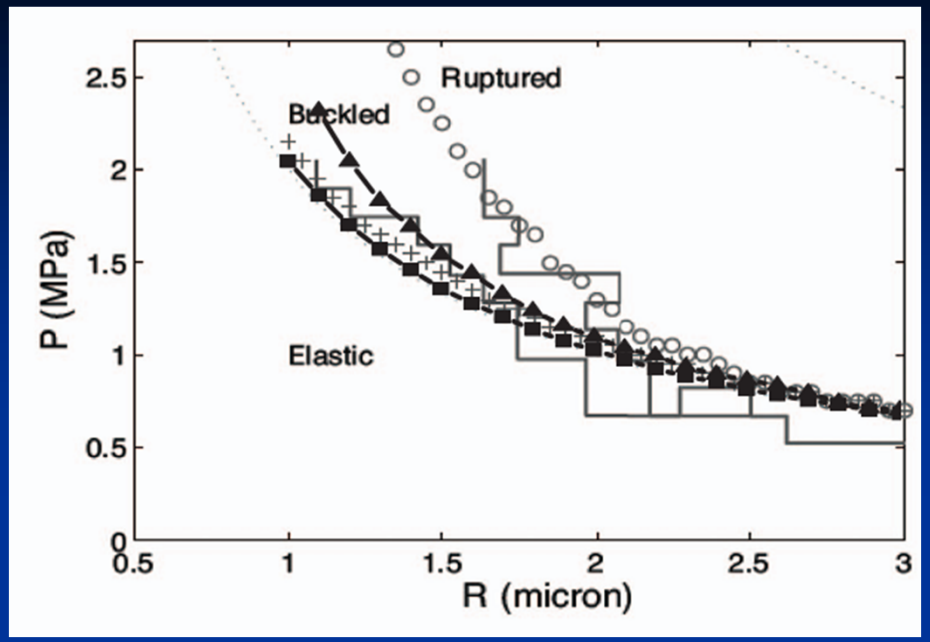

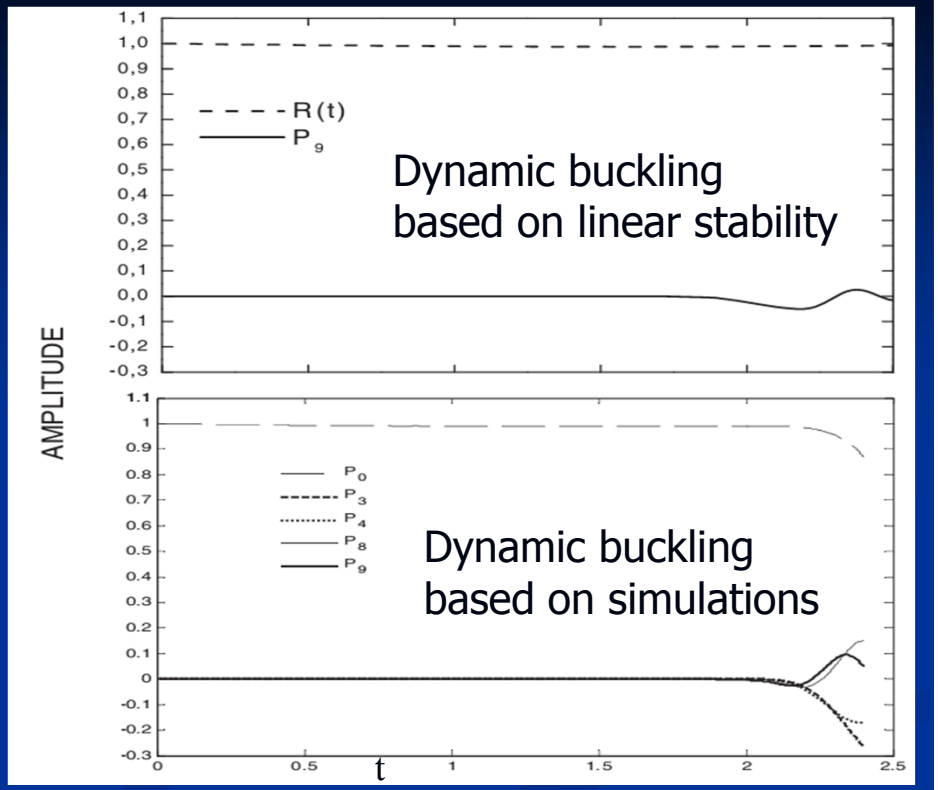

- Lower and upper solid lines -> threshold for buckling and transient break-up based on experiments (Bouakaz et al. 2005)

- Lower dotted line, crosses and solid circles -> buckling threshold obtained via static stability, finite element analysis and surface evolver
- Upper dotted line -> static rupture criterion due to stretching at expansion (too high)
- Open circles -> transient break-up based on the revised Marmottant model (requires unrealistically large shell thickness
- Solid triangles -> Threshold of dynamic buckling based on linear stability and simulatilons

The behavior of polymeric shells, large area dilatation, conforms with the concept of a viscoelastic solid with stretching and bending stiffness

Parametric Stability & Dynamic Buckling for Phospholipid Shells

$R_{eq} = 3.6\ \mu m, G_s = 80\ MPa, \delta = 1\ nm, \mu_s = 20\ Pa \cdot s, b = 0, \nu = 0.5,$
$\rho_l = 998\ kg/m^3, P'_{st} = 101325\ Pa, \gamma = 1.07, \nu_f = 1.7\ MHz, K_{BD} = 3.0d-14\ Nm$

Saturation - Harmonic resonance

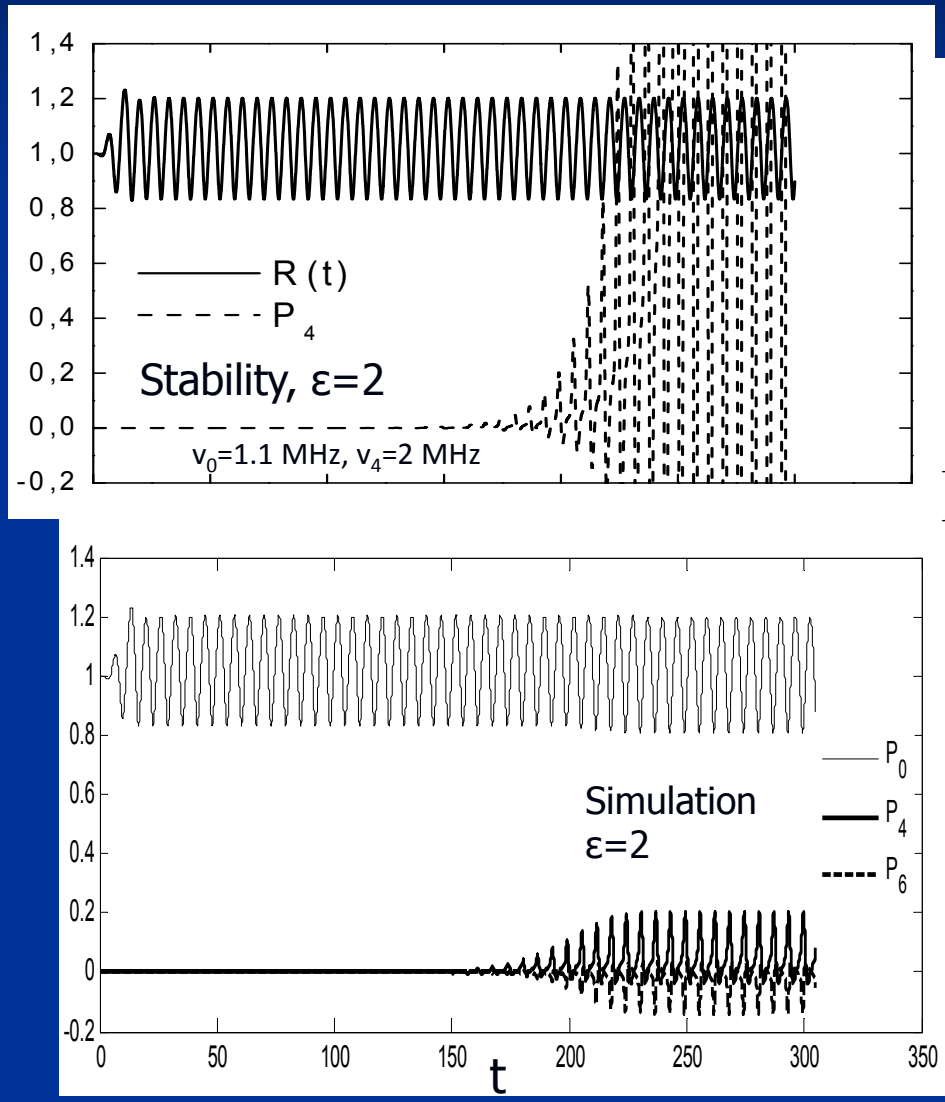

Transient Break-up

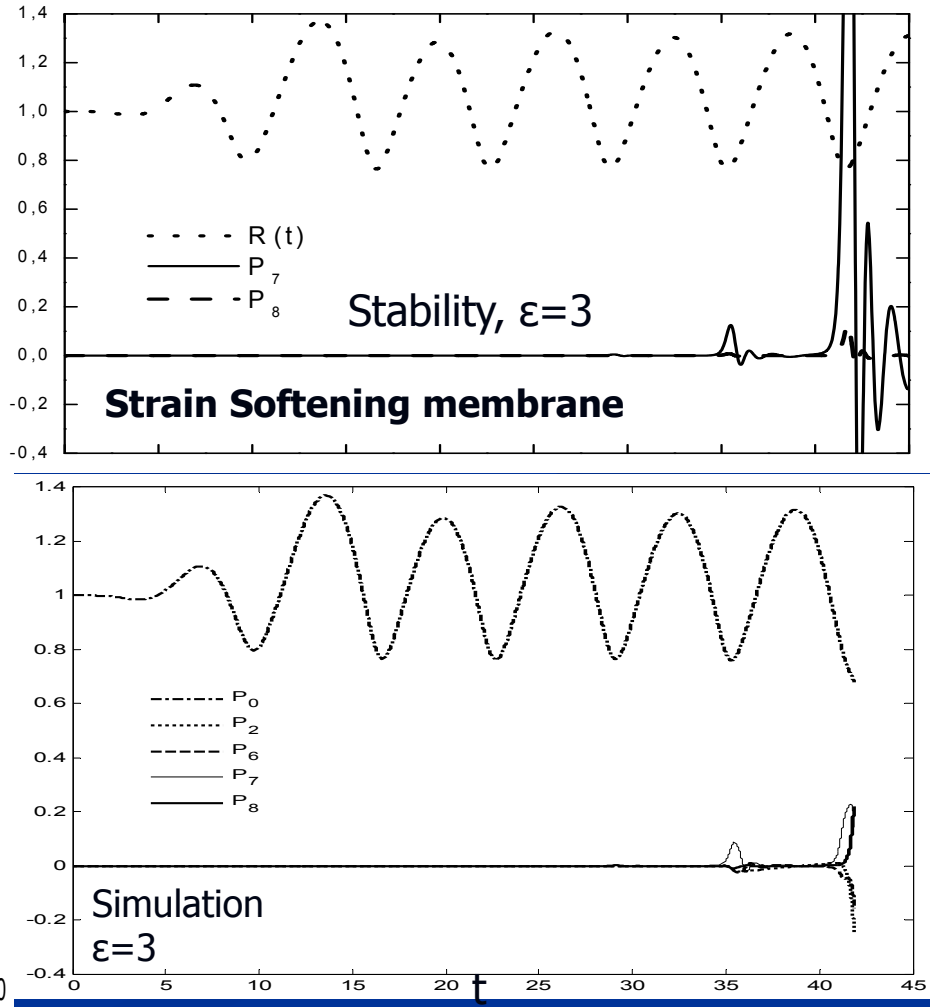

Parametric Stability

$$R_{eq} = 3.6\ \mu m,\ G_s = 80\ MPa,\ \delta = 1\ nm,\ \mu_s = 20\ Pa \cdot s,\ b = 0,\ \nu = 0.5,\ \mu_l = 0,\ C_l \to \infty,$$

$$\rho_l = 998\ {}^{kg}/_{m^3},\ P'_{st} = 101325\ Pa,\ \sigma = 0.051,\ \gamma = 1.07,\ v_f = 3.4 MHz,\ K_{BD} = 3.0d-14 Nm$$

Saturation - Subharmonic Resonance

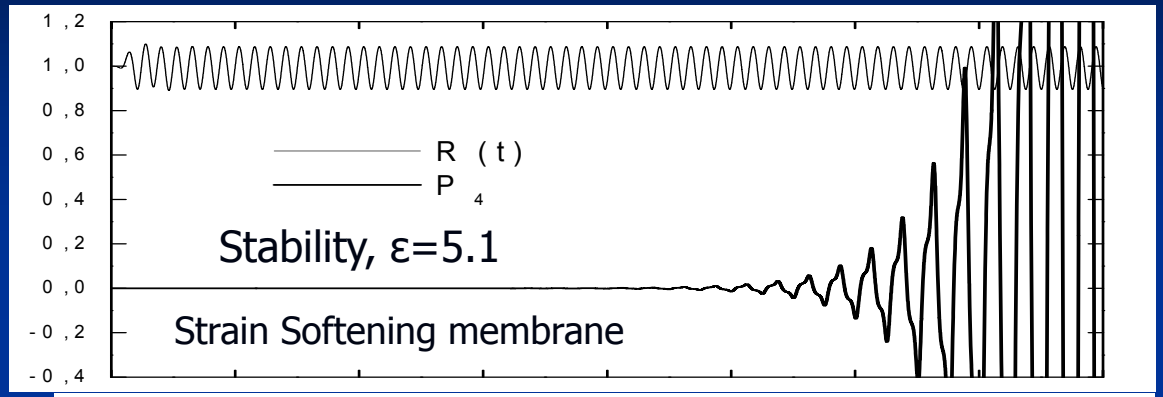

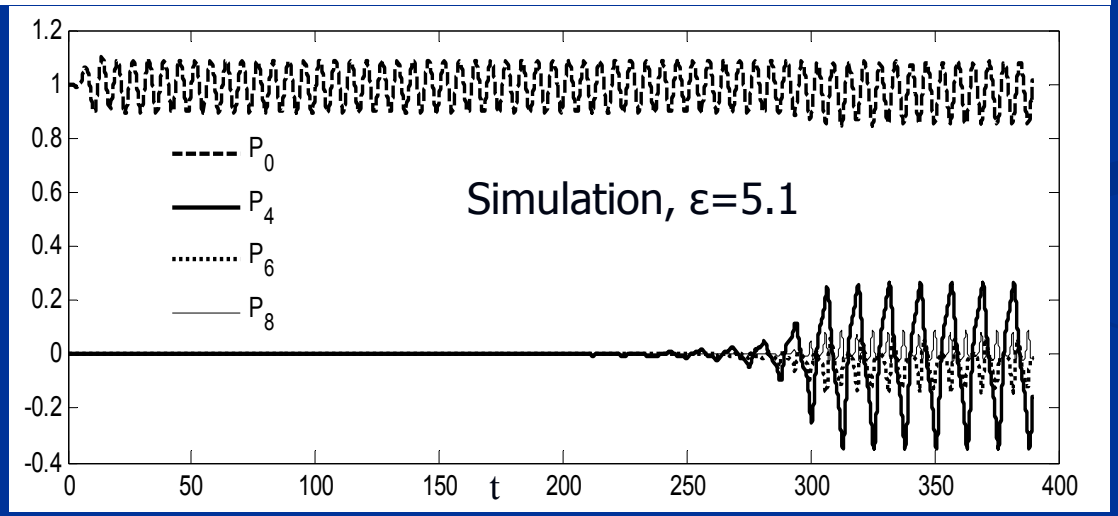

- **In both types of resonance shape modes grow mostly during compression**
- **They reach saturation upon exchanging energy with the radial mode**
- **As the amplitude is further increased towards the threshold of dynamic buckling transient break-up is observed**

- Subharmonic oscillations are more conducive to saturation because there is more time available for the stabilizing effect of energy transfer between modes
- Strain hardening membranes undergo only transient break up either through harmonic or subharmonic resonance

Parametric Stability- The effect of Residual stresses

$R_{eq} = 4.0\ \mu m, G_s = 80\ MPa, \delta = 1\ nm, \mu_s = 20\ Pa \cdot s, b = 0,\ \nu = 0.5, \mu_l = 0, C_l \to \infty,$
$\rho_l = 998\ {}^{kg}/_{m^3}, P'_{st} = 101325\ Pa, \sigma = 0.051, \gamma = 1.07, \nu_f = 1.7 MHz, K_{BD} = 3.0d-14 Nm$

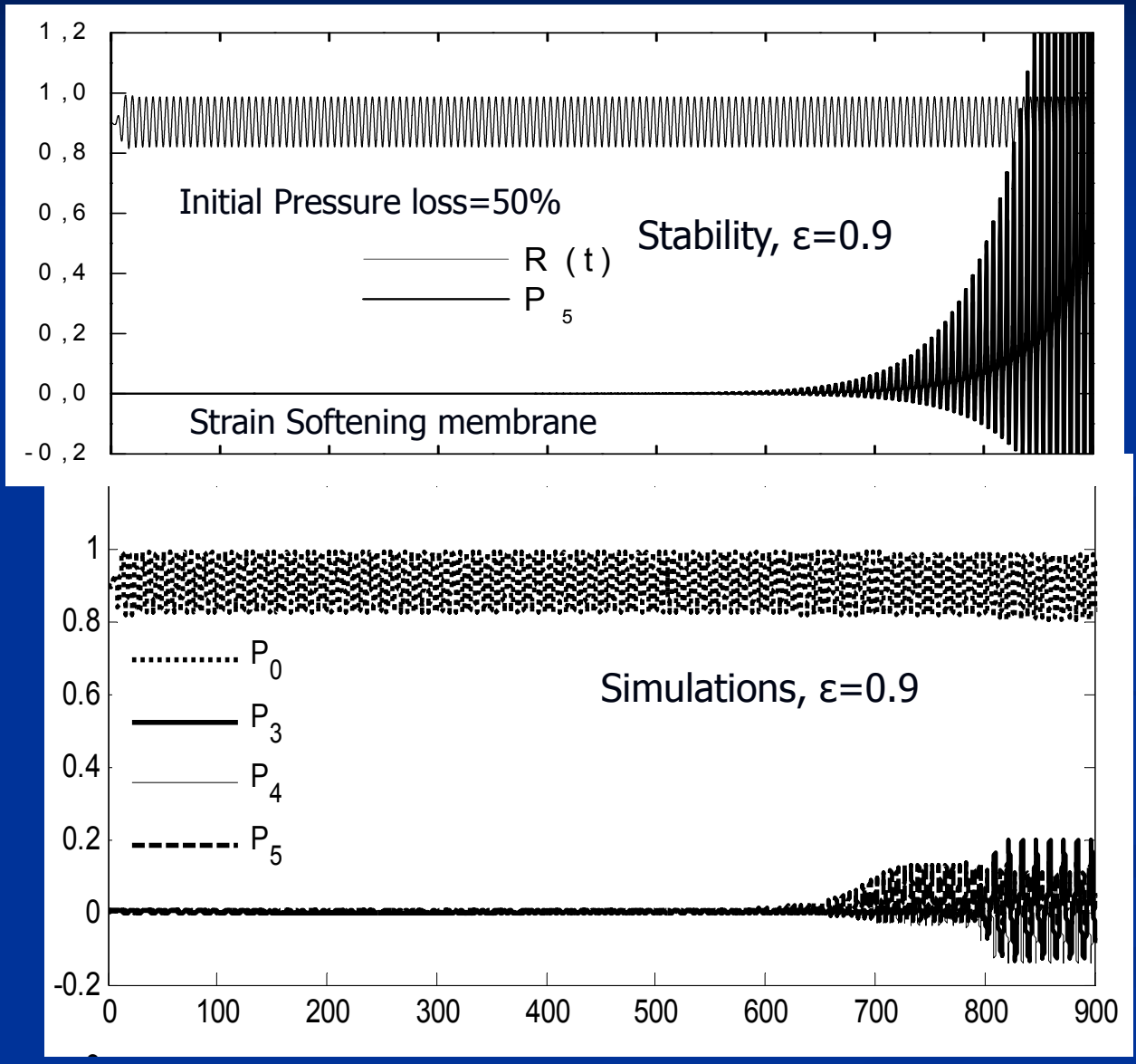

- Residual stresses significantly reduce the stability threshold in terms of sound amplitude
- Shape mode growth occurs primarily during compression
- The amplitude window between saturation and transient break-up is condensed

The effect of Residual stresses – Change in the Constitutive Law

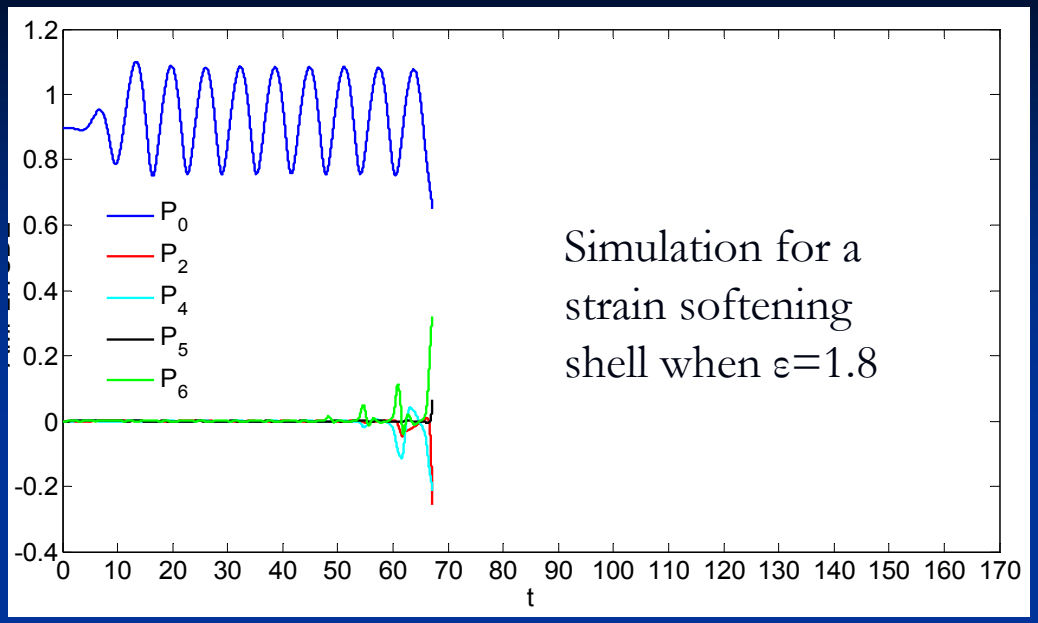

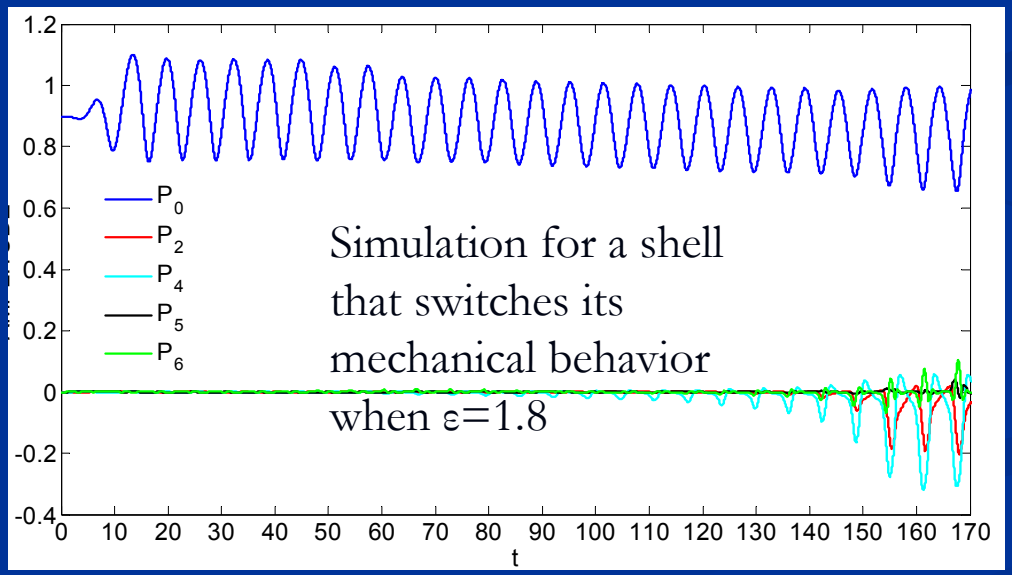

Tsigklifis & Pelekasis, to appear in the Physics of Fluids (2013)

- Increasing ε to 1.5 results in transient break- up of the microbubble via dynamic buckling
- Employing a change in the constitutive law from strain softening to strain hardening results in a compression only type behavior with viscous stabilization of microbubble pulsations
- This phase transition is employed when the amplitude of emerging shape modes grows beyond a certain level signifying the appearance of high curvature regions where lipid bilayers are formed

Dynamic Buckling - Comparison with Experiments

R_{bal}=1.5 μm, ρ_l=998 kg/m^3, P_{st}=1 atm, ν_f=2.4 MHz, ε=12, γ=1.07 , $P_\infty=P_{St}[1+\varepsilon\cos(2\pi\nu_f t)]$

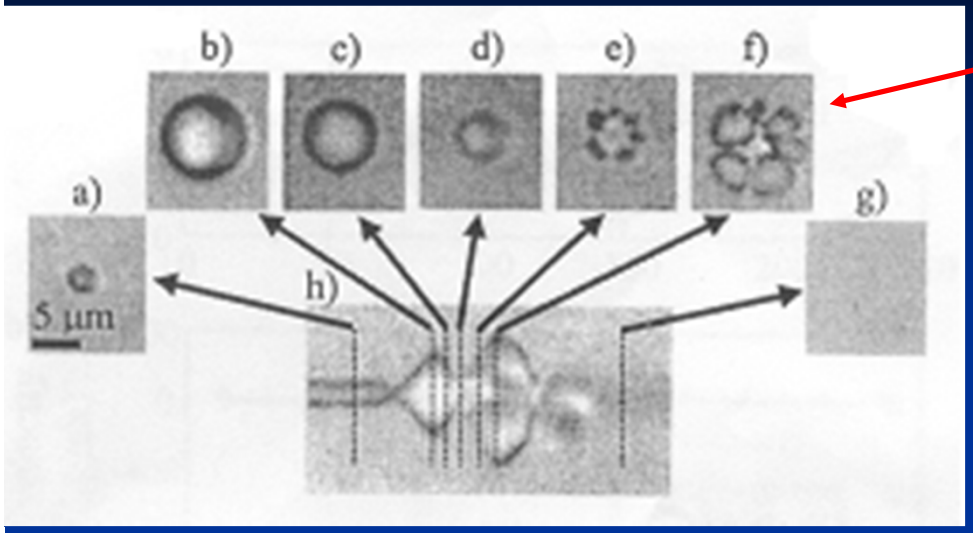

Experimental observations by J. E.Chomas et al. (2004) with MP1950

Break-up is attributed to Rayleigh – Taylor instability

Numerical simulations

- **Assuming a free bubble produces the same maximum volume expansion without observing Rayleigh – Taylor instability**

Considering a membrane described by the Mooney-Rivlin constitutive law, the shell elasticity can be adjusted so that the maximum volume expansion is recovered

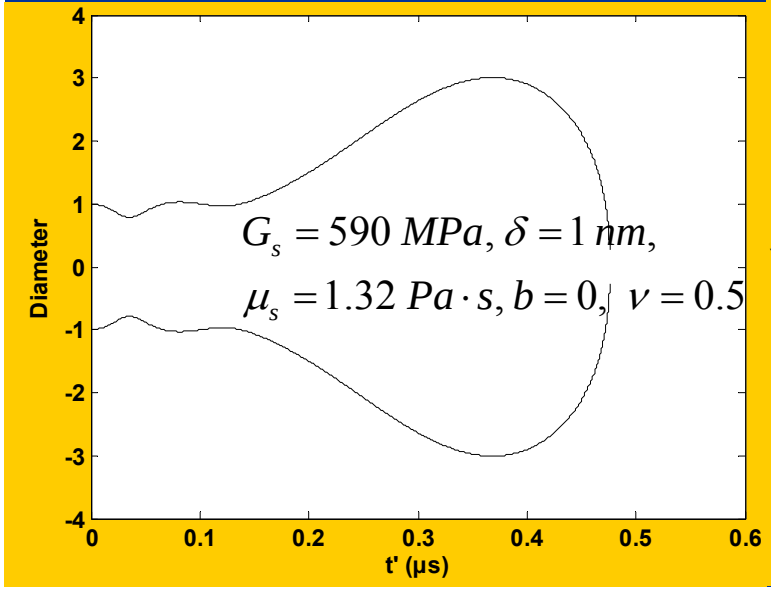

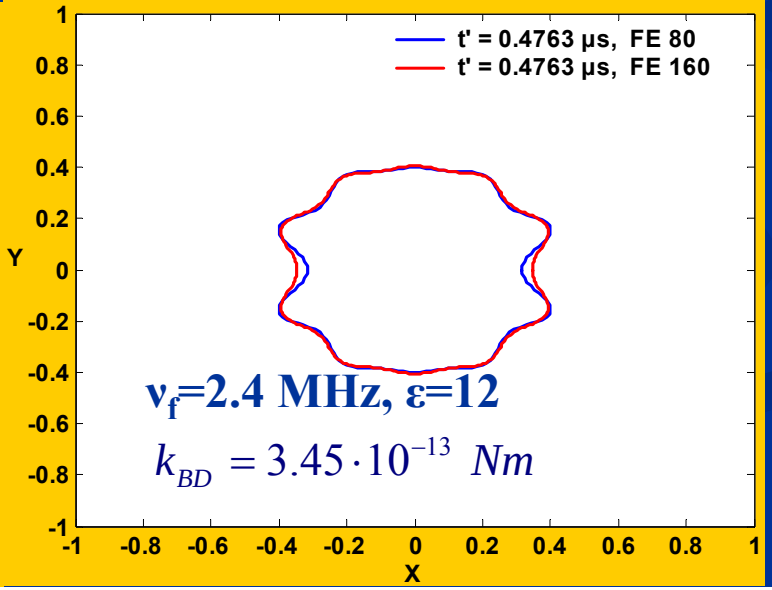

- The microbubble fragments very fast via dynamic buckling
- The time to fragmentation is controlled by bending resistance kB and shell viscosity
- Simulations recover predictions of stability analysis

Static Response

- Need to dissociate static from dynamic effects in order to extract the mechanical properties of the shell
- Static measurements will allow phase transitions and folding instabilities to manifest themselves
- Alternative means, to acoustic measurements, for obtaining parameter estimates
- Typically the linear regime provides the shell stiffness for given shell thickness h
- For very thin phospholipid shells h is not known and k_b is a more appropriate independent parameter

Finite Element Simulations

- Solution of the normal and tangential force balance along with the torque balance for a shell of small but finite thickness – Point or distributed loads are considered
- The effect of gas compressibility is also considered
- Effects of cantilever stiffness and curvature are also important

AFM Measurements with Contrast Agents

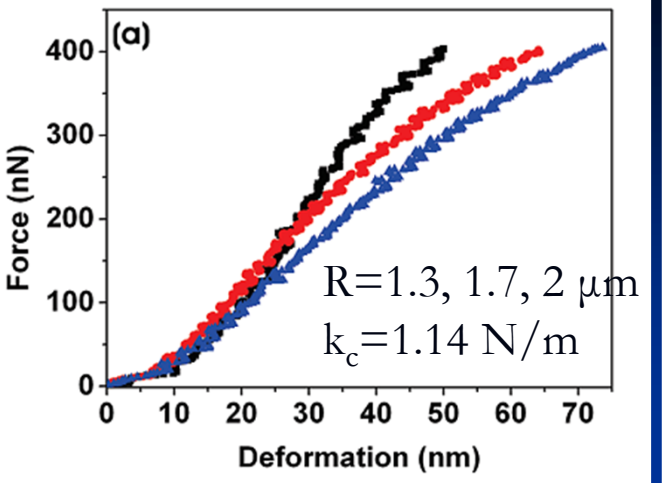

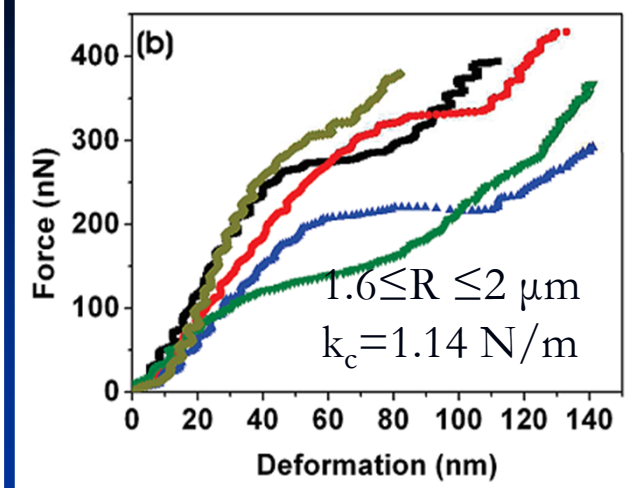

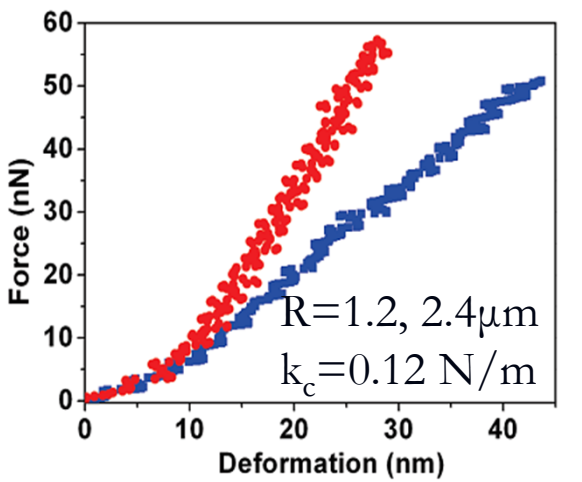

AFM measurements of polymer microspheres (bisphere) with tipless cantilevers of varying stiffness, k_c (Glynos et al. Langmuir, 2009)

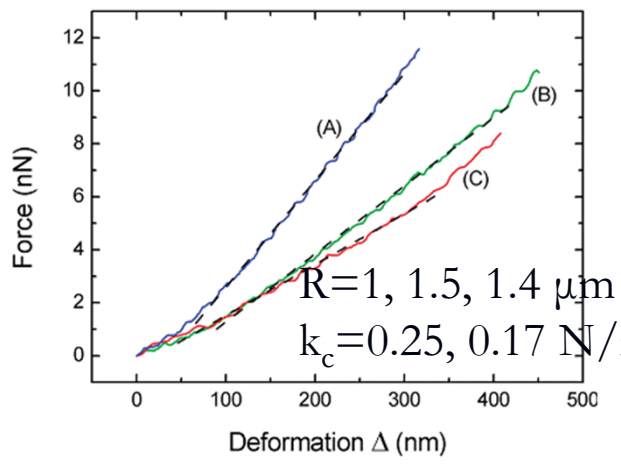

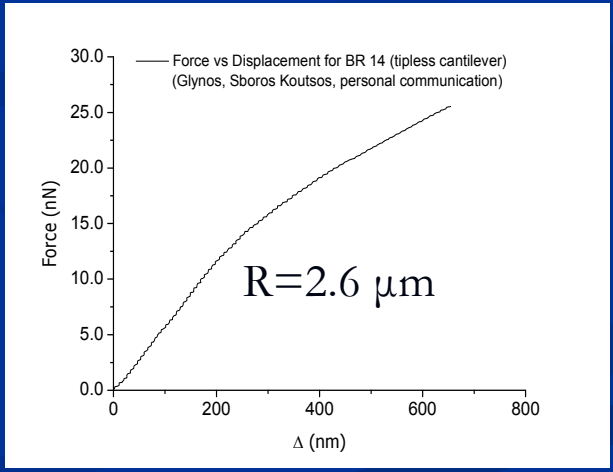

AFM measurements of phospholipid shells (definity and BR14) with tipless cantilevers of varying stiffness, k_c (Santos et al. Langmuir, 2012)

Axisymmetric Static Deformation

Schematic of an AFM setup for compression of single hollow microsphere with a cantilever

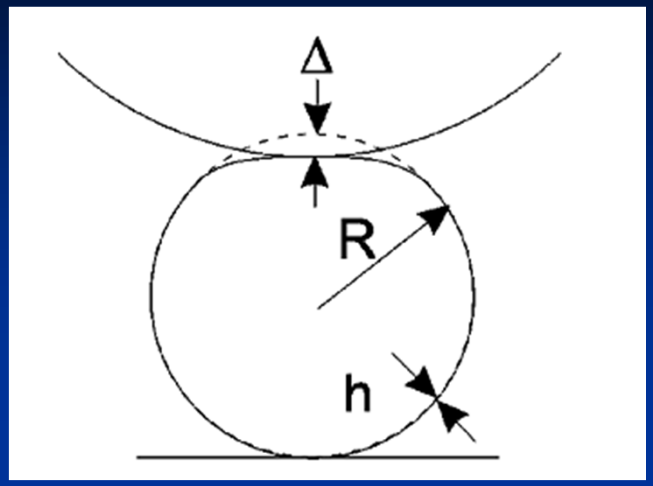

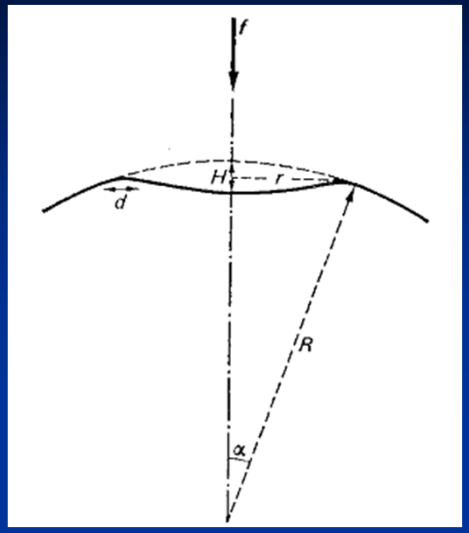

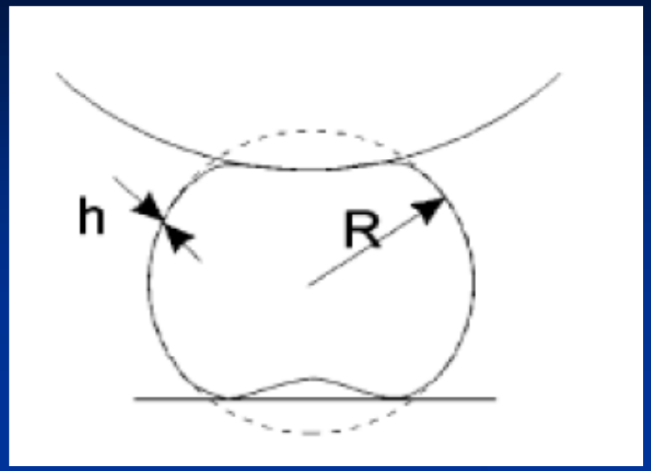

Linear regime (Reissner): $F = \frac{8G_s h^2}{R}\Delta$ Nonlinear regime (Pogorelov): $F = \frac{\sqrt{3.56}\cdot 3G_s h^{5/2}}{(1-\nu^2)R}\Delta^{0.5}$

- The balance between stretching and bending energies (a) for the case of a flattened shell and (b) when a crater is formed at the pole provides the linear (Reissner) and nonlinear (Pogorelov) force-deformation relation
- An estimate of bending and stretching elasticities is pursued based on asymptotic analysis of the experimental force displacement curve
- In principle, fitting the experimental data with the above two types of behavior may produce both area dilatation and bending resistance of the shell

Data Analysis

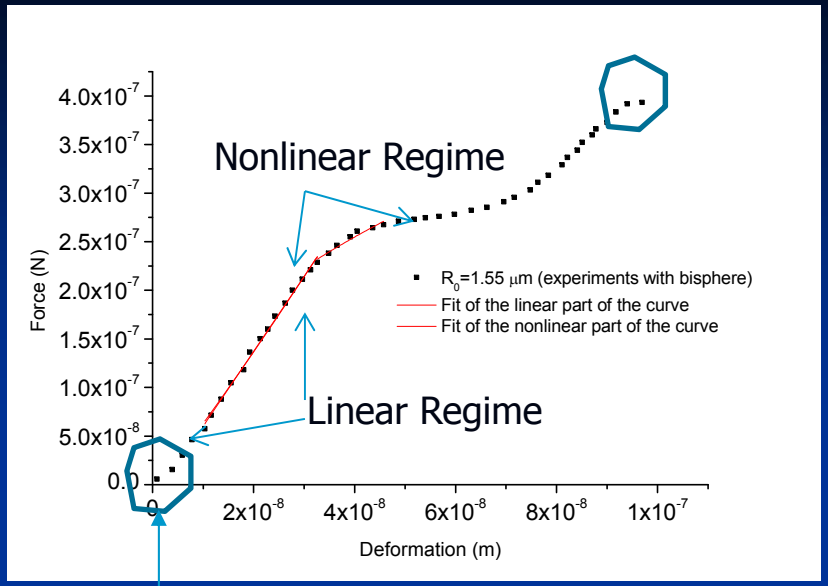

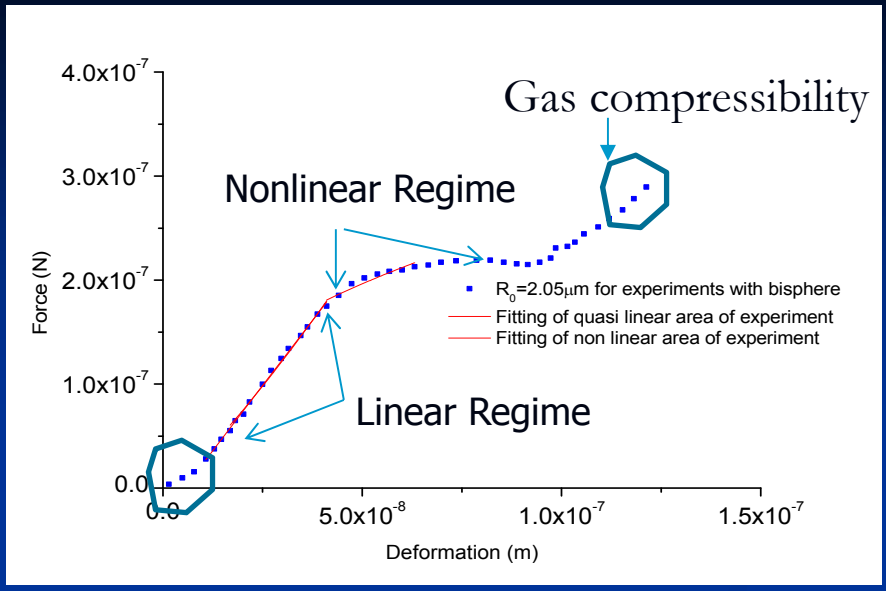

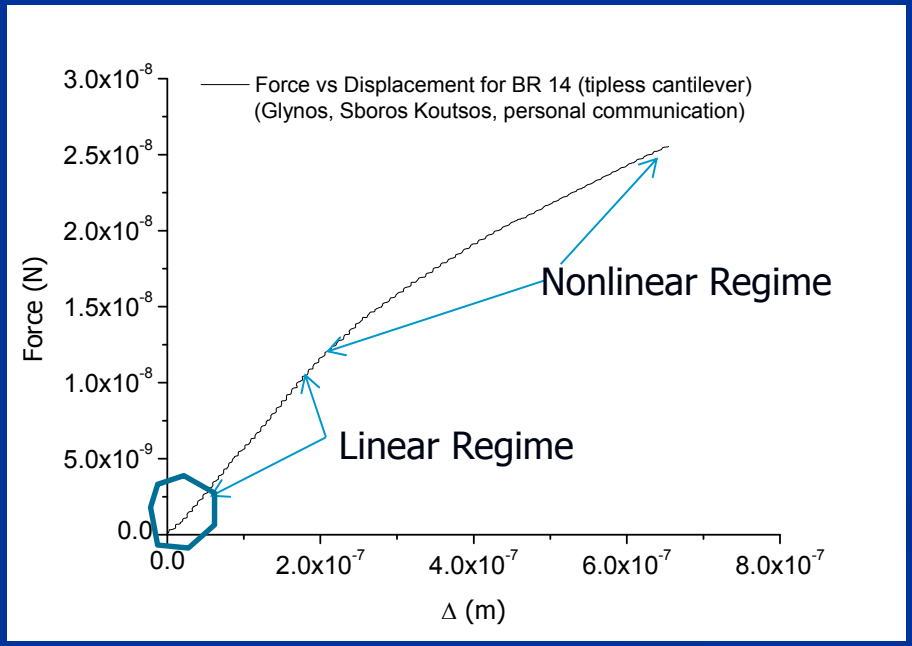

Overall Picture

- At very low forcing attractive adhesive forces balance elastic forces
- Linear part is characterized by stretching and bending forces
- Ensuing nonlinear part behaves like $F \sim \Delta^{0.5}$ and is chacterized by a narrow rim of deformation
- At large deformations abrupt increase of forces is needed in order to account for added stiffness due to compressibility of enclosed gas (for soft shells)
- Phase transitions and instabilities

Static Simulations of Microbubble Response to a Point Load

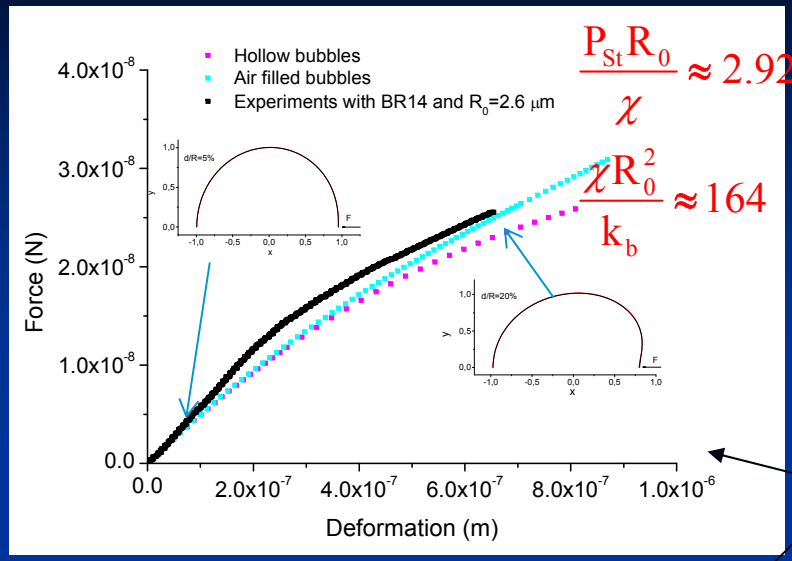

- Coupling of experimental data from the two regimes with asymptotic prediction provides estimates of $\chi=3G_sh$ and k_b to be used in the simulations
- For BR14 we obtain $\chi\sim0.1$ N/m and $k_b\sim0.5\times10^{-14}$ N·m – Using χ and h instead would obtain an unrealistic value for h

Phospholipid shells

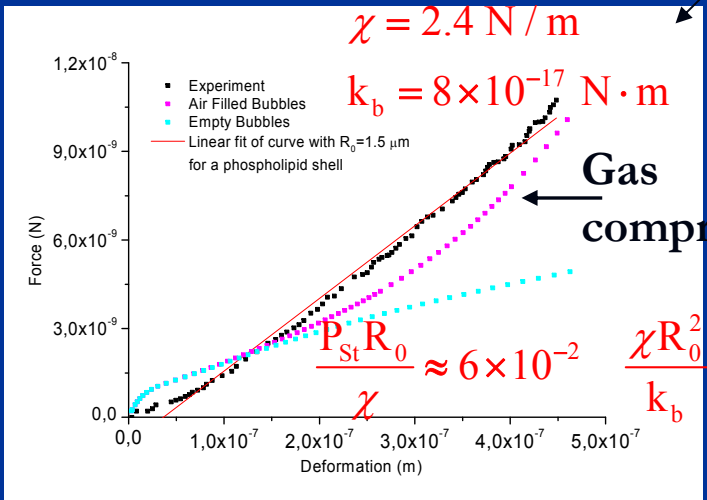

Failure to capture initial regime may compromise accuracy in certain cases

Polymeric shell

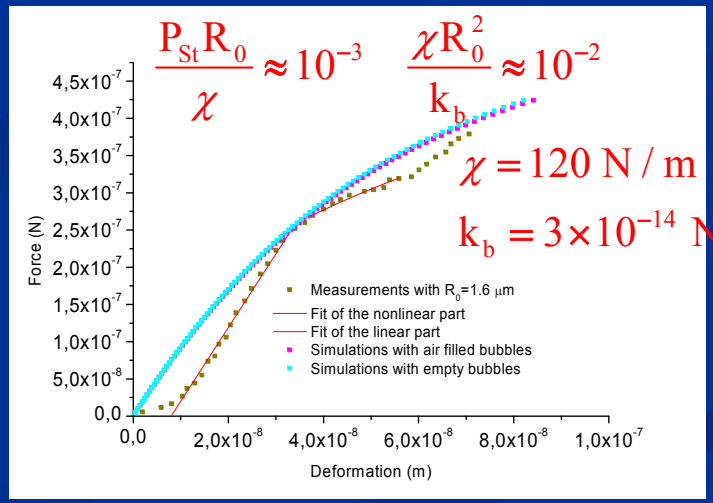

Cantilever curvature and deformability is also a factor

Conclusions

- Nonlinear shell properties, e.g strain softening vs. strain hardening membrane material, significantly affect contrast agent response

  Allowing for bending elasticity shape deformation and buckling are captured
  Bending elasticity is independent from area dilatation modulus due to non-isotropy of the membrane

  Polymeric shells follow a **neo-Hookean** behavior - **Lipid monolayer** shells exhibit a **strain softening behavior** (they become softer at expansion as the area density of the monolayer decreases) – **Lipid bilayer** shells exhibit **strain hardening** behavior (they become softer at compression)

- Static buckling occurs when the microbubble suffers a step increase in external pressure, or a sinusoidal change of very small frequency compared against its resonance frequency, of sufficiently large amplitude

  Static simulations of point load response reveal linear and nonlinear regimes that can be combined to provide estimates of χ and k_b

  Shell thickness is not a relevant parameter for thin monolayer shells
  Compressibility effects will improve estimates for shells with stiffness that is comparable with stiffness due to gas compressibility, e.g. lipid monolayers

  Important parameters $\frac{P_{St} R_0}{\chi}, \quad \frac{\chi R_0^2}{k_b}$

  Adhesion forces at small deformations and cantilever deformability are expected to also play a role

- With the available modeling tools a number of dynamic effects exhibited by contrast agents is understood and captured, e.g. resonance frequencies, abrupt vibration onset, rich harmonic content, expansion and compression only behavior, harmonic and subharmonic shape mode excitation
- Mode saturation is captured above the stability threshold (supercritical growth) for parametric excitation -- Growth of unstable modes occurs mostly during compression -- Part of the energy lost by the radial mode due to deformation is returned to it via nonlinear interaction with the emerging mode during compression $\rightarrow$ Preferential radial excursion at compression
- Strain softening shells exhibit this pattern more often and mostly for subharmonic ecxitation for which there is more time available for energy exchange – As the amplitude increases towards the threshold for dynamic buckling transient break-up takes place
- Dynamic buckling (equivalent to Rayleigh-Taylor instability for free bubbles) occurs exponentially fast for much larger sound amplitudes
  Strain softening shells tend to exhibit this behavior at lower amplitudes than strain hardening ones due to viscous stabilization of the latter

- "Compression only" behavior is probably associated with bending at compression and subsequent formation of bilayer structures that introduce strain hardening behavior to the shell response → Results in significant radial excursion at compression and stabilization, against growth of shape modes and transient break-up, due to viscous damping

  For an initially pre-stressed shell the amplitude thresholds for parametric mode excitation and transient break-up are significantly reduced and the window for saturated pulsations shrinks – "Compression only behavior" is a natural means to extend the stability and cohesion of the microbubble

Current & Future Work

- Develop a constitutive law for bending and stretching energy that is taylor-made for each contrast agent and accounts for monolayer to bilayer phase transitions
- Develop a set of static, e.g. via AFM, and dynamic measurements for contrast agent characterization
- Study Bubble-wall, bubble-cell interaction and the dynamic behavior of trapped microbubbles

Thank you for your attention

Questions